Energy & Environmental Science

Accepted Manuscript

Exciton Diffusion in Organic Semiconductors

Oleksandr V. Mikhnenko,*[a] Paul W. M. Blom,*[b] Thuc-Quyen Nguyen*[a,c]

[a]Center for Polymers and Organic Solids and Department of Chemistry and Biochemistry, University of California, Santa Barbara, CA 93106

[b]Max Planck Institute for Polymer Research, Ackermannweg 10, 55128 Mainz, Germany

[c]Department of Chemistry, Faculty of Science, King Abdulaziz University, Jeddah, Saudi Arabia

Email: alex@mikhnenko.com, blom@mpip-mainz.mpg.de, quyen@chem.ucsb.edu

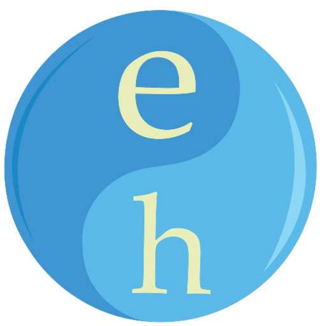

TOC

Experiments and basic Physics of exciton diffusion in organic semiconductors are reviewed.

Broader context

Organic semiconductors provide emerging technology for consumer electronics. Organic light emitting diodes (OLEDs) have already entered the market as they offer more vibrant colors when compared to conventional liquid crystalline screens. Organic photovoltaics (OPV) promise flexible and inexpensive solar cells, which will find niche applications for smart power generation such as clothing, portable cellphone charges, and power generating windows. These devices convert electricity to light and light to electrical current using excited states called excitons. Dynamics of excitons determine key device performance characteristics such as power conversion efficiency of solar cells and brightness of OLEDs. This review summarizes recent experimental findings and basic concepts relevant to exciton diffusion in organic semiconductors.

Abstract

The purpose of this review is to provide a basic physical description of the exciton diffusion in organic semiconductors. Furthermore, experimental methods that are used to measure the key parameters of this process as well as strategies to manipulate the exciton diffusion length are summarized. Special attention is devoted to the temperature dependence of exciton diffusion and its relationship to Förster energy transfer rates. An extensive table of more than a hundred measurements of the exciton diffusion length in various organic semiconductors is presented. Finally, an outlook of remaining challenges for future research is provided.

Biographies of authors

Oleksandr V. Mikhnenko is a postdoctoral scholar in the group of Prof. Nguyen at University of California Santa Barbara. He received his PhD degree from University of Groningen in the lab of Prof. Maria A. Loi and Prof. Paul W.M. Blom. Oleksandr is interested in fundamental properties of organic semiconductors as well as in Physics of unconventional electronic devices.

Paul W. M. Blom, born in 1965 in The Netherlands, received his Ph.D. Degree□in 1992 from the Technical University Eindhoven on picosecond charge-carrier dynamics in GaAs. At Philips Research Laboratories he was engaged in the electro-optical properties of polymer light-emitting diodes. From 2000, he held a professorship at the University of Groningen in the field of electrical and optical properties of organic semiconducting devices. In September

2008, he became Scientific Director of the Holst Centre in Eindhoven, where the focus is on foil-based electronics, followed in 2012 by an appointment as director at the MPI for polymer research.

Thuc-Quyen Nguyen is a professor in the Center for Polymers & Organic Solids and the Chemistry & Biochemistry Department at University of California, Santa Barbara (UCSB). She received her Ph.D. in physical chemistry from the University of California, Los Angeles, in 2001. She was a research associate in the Department of Chemistry and the Nanocenter at Columbia University. In 2004, she began her independent career at UCSB. Her current research interests are structure-function-property relationships in organic semiconductors, electronic properties of conjugated polyelectrolytes, interfaces in optoelectronic devices, charge transport in organic semiconductors and biological systems, organic solar cells, and device physics.

Table of Contents

1. Introduction

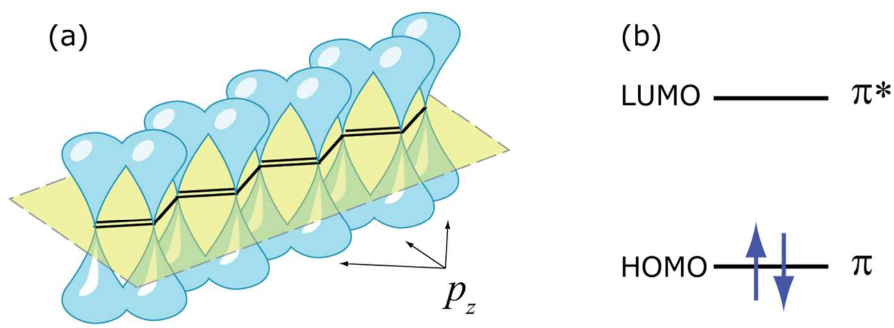

Figure 1: (a) A conjugated backbone with overlapping p_z orbitals that point out of the molecular plane. **(b)** Highest occupied and lowest unoccupied molecular orbitals (HOMO and LUMO). Arrows denote two electrons with different spins.

Organic semiconductors are carbon-based compounds that show semiconducting properties. Alternation of single and double bonds between carbon atoms – conjugation – is a common structural property of all organic semiconductors. This zigzag backbone usually adopts a planar conformation (**Figure 1a**). Covalent bonds between carbon atoms of such a backbone are formed by three sp^2 hybridized orbitals and one unhybridized orbital, which is commonly denoted as p_z (Ref. [1]). Unhybridized orbitals p_z provide electron clouds above and below the molecular plain. The adjacent p_z orbitals overlap resulting in shared molecular orbitals that are often referred as extended π-system. Electrons on these orbitals are spatially delocalized meaning that they belong to the whole π-system, but not to specific carbon atoms. A π-system can be extended over the entire organic molecule or just over a part of it – a conjugated segment.

In the ground state, electrons fill orbitals of the lowest energies with maximum two electrons of opposite spins per each orbital. The energetically highest occupied and the lowest unoccupied molecular orbitals (HOMO and LUMO) are very important for electrical conductivity and optical properties of organic semiconductors. They are often denoted as π and π* orbitals in π-systems, respectively (**Figure 1b**). The energy difference between HOMO and LUMO is often referred as a band gap that typically values between 1.5 and 3.5 eV for organic semiconductors.

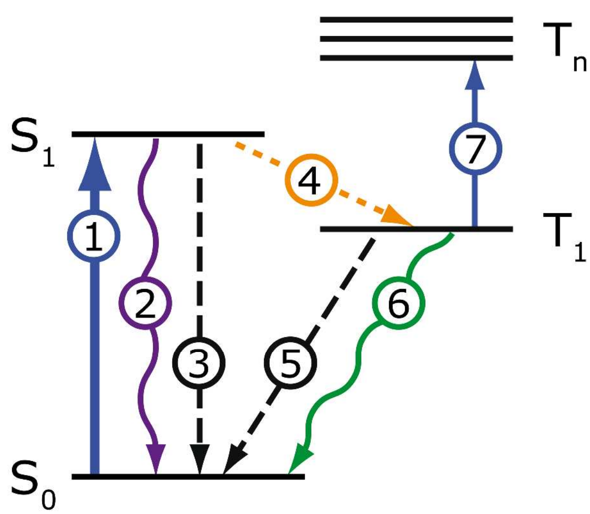

Figure 2: The Jablonski diagram of electronic transitions in organic semiconductors. The energies of singlet (S_0 and S_1) and triplet (T_1 and T_n) states are scaled vertically. Absorption (1), fluorescence (2), intersystem crossing (4), phosphorescence (6), nonradiative transitions (3 and 5) and photoinduced absorption (7) are presented as arrows.

Excitons are Energy Chunks

The ground state of the majority of organic molecules is electrically neutral and has net spin zero. A molecule can be excited when an electron from the HOMO is promoted to the LUMO, for instance by absorption of a photon. The Jablonski diagram in **Figure 2** presents possible transitions between electronic states of an isolated molecule. These states are positioned vertically by their energy and grouped horizontally by spin multiplicity. Electronic states with net spin zero or one are called singlets or triplets, respectively. The arrow **1** represents the absorption of a photon that brings a molecule from the ground state S_0 to the first singlet excited state S_1; transitions to higher singlet excited states are also possible (not shown in **Figure 2**). The transition **2** results in the emission of light and is called fluorescence. Triplet excited state T_1 can be created via the intersystem crossing **4**. The radiative transition **6** is called phosphorescence. Fluorescence and/or phosphorescence can be also referred as photoluminescence (PL) when these transitions are initiated by absorption of a photon. The non-radiative transitions **3** and **5** compete with fluorescence and phosphorescence. And finally transition **7** is the absorption of a photon that brings state T_1 to higher triplet excited states T_n. This process can be used to detect triplet excitons in photoinduced transient absorption experiments.[2] In some cases a singlet exciton can undergo a fission process resulting in two triplet excitons.[3–14] For details on singlet fission please refer to review papers specified in references.[15–18]

In organic solids, interactions of an excited molecule with neighbors impose reorganization of intermolecular distances and partial polarization of electronic configuration of the surrounding. This collective response to an excitation is called exciton or, in case of particularly strong interactions with surrounding, exciton-polaron.[19,20] Excitons are electrically neutral and bear potential energy that can be released when the molecule returns to the ground state. Excitons with total spin of *zero* or *one* are called singlet or triplet, respectively. Although the Jablonski diagram in Figure 2 describes isolated molecules, transitions in organic solids are usually similar. Therefore singlet and triplet excitons are often denoted as S_1 and T_1.

Two charged states – positive or negative polarons – can be created by subtraction from the HOMO or addition to the LUMO of an electron, respectively. Polaron entities include the charge and reorganization energy of the surrounding. Terms "hole" and "electron" are often used to denote positive and negative charges. An exciton can be described as a bound electron-hole pair, which is localized at a single conjugated segment. Such localization is due to relatively low dielectric constant of the organic medium resulting in a strong electrostatic attraction between the opposite charges. Furthermore, the excitonic wavefunction is usually localized at a single conjugated segment due to weak interactions between molecules in organic solids. The work needed to separate electron and hole of an exciton is called binding energy and is usually of the order of 0.3-0.5 eV for singlet excitons.[21–23] The binding energy of triplets is higher due to the attractive exchange interaction between electron and hole of the same spin orientation.[2]

Triplet excitons cannot be directly generated by the absorption of a photon in organic semiconductors due to symmetry considerations of π orbitals. Thus the assistance of spin-orbit coupling and/or electron-phonon interaction are required to enable transitions such as the **4**, **5** and **6** in Figure 2. Organic semiconductors are composed of lightweight atoms such as carbon, hydrogen, oxygen, nitrogen and sulfur, which do not show strong spin-orbit coupling. Consequently, the transitions between excitonic states of different spin multiplicity are normally not efficient in this class of materials. Therefore triplet lifetime is usually about 6 orders of magnitude longer than that of singlets in organic semiconductors.

As a rule of thumb, the energy that is carried by a triplet exciton is usually 0.7 eV below that of singlet in a π system.[2] However, it is also possible to design conjugated molecules that have similar singlet and triplet energies.[24,25] In such systems the intersystem crossing **4** and the reverse process is more likely to occur and these molecules show a phenomenon of temperature activated delayed fluorescence (TADF). Please refer to [26,27] for detailed review on TADF compounds.

Energy and Charge Transfer

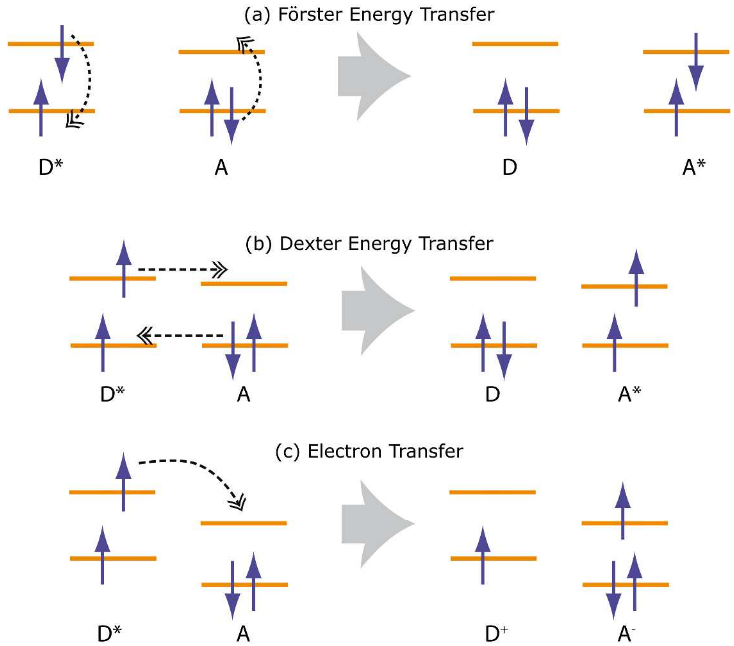

Figure 3: **(a)** Förster energy transfer. **(b)** Dexter energy transfer enables diffusion of triplet excitons. The horizontal lines are HOMO and LUMO energy levels of donor (D) and acceptor (A) molecules; the asterisk denotes excited state. The dashed arrows represent simultaneous rearrangement of the electronic configuration. **(c)** Electron transfer from an excited donor molecule (D*) to a neutral acceptor (A).

An exciton can be relocated from an exited "donor" molecule to an "acceptor" molecule via a non-radiative process of energy transfer. At the end of this process the donor molecule is in the ground state and the acceptor molecule is in the excited state. Energy transfer can occur via Förster (through-space) or Dexter (through-bond) mechanisms (**Figure 3a** and **b**).[28–30] The Förster mechanism is based on a dipole-dipole electromagnetic interaction and occurs when the emission spectrum of the donor has a significant overlap with the absorption spectrum of the acceptor. Therefore, this type of energy transfer is called Förster *resonant* energy transfer (FRET). The efficiency of FRET decreases with the distance r between donor and acceptor as r^{-6}. Significant FRET can be typically observed for donor-acceptor separations in the range of 1-5 nm.[30–32] Usually, only singlet excitons can be transferred via the Förster mechanism; however, a triplet exciton that is located at a phosphorescent donor also can undergo FRET.[33–38] Förster energy transfer is commonly observed in photosynthesis when the energy of absorbed photons is channeled to the reaction center.

Actual exchange of electrons between donor and acceptor takes place during the Dexter energy transfer (**Figure 3b**).[2,28,30] This may happen when donor and acceptor are only about 1 nm apart so there is a significant overlap of molecular orbitals. The probability of Dexter energy transfer exponentially decreases with the distance between donor and acceptor. Both singlet and triplet excitons may be transferred by this mechanism. FRET usually outperforms the efficiency of the Dexter energy transfer for singlet excitons, while triplets may be transferred between non-phosphorescent molecules only by the Dexter mechanism.

Electron and hole, which are coulombically bound in an exciton, can be separated when their binding energy is overcome. Such a separation can be efficient at the interface with an electron accepting material. If the energy of the LUMO of the acceptor is significantly lower than the LUMO of the excited donor molecule, then electron transfer from donor to acceptor may take place (see **Figure 3c**). This process is called charge transfer; it is a short-range interaction that takes place when there is a significant spatial overlap between wavefunctions of the donor and acceptor molecules. As a result of the electron transfer donor and acceptor are positively and negatively charged, respectively. Hole transfer is also possible when the energy levels of a donor and an acceptor are properly aligned. The physical mechanism of this process is the same as that of the electron transfer.

Excitons in Opto-Electronic Devices

The working principle of organic light emitting diodes (OLEDs) is based on the generation of excitons. Electrons and holes are injected into an organic semiconductor, which serves as active layer for the OLED. Excitons are created when electron and hole meet each other in the active layer. According to the quantum mechanical rules of momentum addition, 25% of all excitons created in this way are singlets and 75% are triplets. The radiative recombination of triplet excitons is not very probable, thus only singlet excitons may contribute to the emitted light that limits the internal quantum efficiency of an OLED to 25%.[2,39] In some materials with low charge carrier mobility, the formation of singlet excitons may be somewhat more or less favorable due to the hyperfine fields, which are caused by magnetic field of hydrogen nuclei.[40–49] Nevertheless, in order to achieve highly performing OLEDs triplet excitons should be manipulated toward radiative recombination.[2,50–54] In this respect, it is highly important to study the dynamics of both singlet and triplet excitons in order to improve the performance of organic OLEDs.

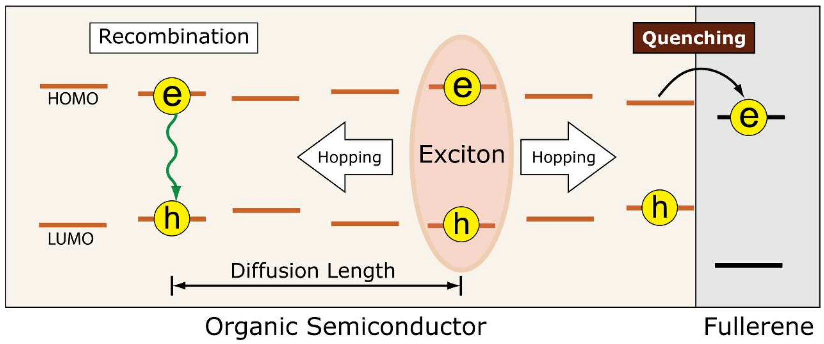

Figure 4: Exciton quenching due to charge transfer at the semiconductor (donor) – fullerene (acceptor) interface. Electrons and holes are denoted as (e) and (h). Conjugated segments are schematically depicted as pairs of HOMO-LUMO levels.

Semiconductor (donor) -fullerene (acceptor) heterojunctions are commonly used in organic solar cells to separate electrons and holes.[55–62] In the simplest case the active layer of an organic solar cell consists of a bilayer semiconductor-fullerene heterojunction (**Figure 4**). The semiconductor plays the role of a light absorber in which singlet excitons are generated fairly homogeneously within the layer. The excitons undergo diffusion so that some of them will reach the interface with the fullerene, where the electron and hole are separated. These electrons and holes are then transported through the fullerene and organic semiconductor layer, respectively, and then extracted at the metallic electrodes of the solar cell resulting in a photocurrent. Excitons that are capable of reaching the fullerene interface may undergo dissociation. Therefore, the exciton diffusion length L_D sets the geometrical constraints on the useful thickness of the semiconductor layer. Excitons that are created at longer distance than L_D from the fullerene interface will not make a contribution to the photocurrent. Terao *et al.* showed an almost linear correlation between the short circuit current of a bi-layer solar cell and the exciton diffusion length.[63] Menke et al. demonstrated that the power conversion efficiency of a bi-layer solar cell can be increased by 30% when exciton diffusion length is manipulated towards larger values.[64]

Singlet exciton diffusion length of organic semiconductors typically falls into range of 5-10 nm (see Table I), however a layer thickness of 100-200 nm is needed to efficiently absorb light. Therefore instead of bi-layer structures, bulk heterojunction solar cells are now routinely prepared. In these devices donor and acceptor materials are intermixed usually by dissolving the two materials in an organic solvent. When a film is cast from such a solution, the resulting phase separated morphology is quite complex and it is called bulk heterojunction. It has been shown that due to diffusion-limited exciton dissociation, a gradual reduction of the short circuit current is observed in a bulk heterojunction solar cell when the morphology was coarsened by means of thermal annealing.[64] On the other hand, devices with optimal morphology, which is characterized by the phase separated domains of the order of 10 nm, are nearly insensitive to variations of exciton diffusion length.[65] Unfortunately it is quite hard to achieve such optimal morphology in practice. Thus for the design efficient solar cells it is important to measure and control the exciton diffusion length.

2. Mechanism of Exciton Diffusion

In this section we focus on main Physical processes that are relevant for exciton diffusion. For vigorous theoretical description of exciton transport please refer to these excellent reviews [2,18,23,66] and other peer-reviewed publications.[67–87]

Diffusion Equation

Diffusion is a random motion of particles in space that leads to spreading from the areas of high concentration to the areas of low concentration. Normal diffusion can be described by the following equation:

$$\frac{\partial n}{\partial t} = D\nabla^2 n - \frac{n}{\tau}, \quad (1)$$

where n is the concentration of particles, D is a diffusion coefficient, ∇^2 is Laplace operator, and τ is the particle lifetime. The root mean square displacement of a particle from its initial position due to the diffusion process is called diffusion length, which is given by:

$$L_D = \sqrt{\frac{\sum dL_i^2}{N}} = \sqrt{2ZD\tau}\ , \quad (2)$$

where dL_i is the displacement of an exciton i from its original position, N is total number of excitons, and Z is equal to 1, 2 or 3 in case of one-, two- or three-dimensional diffusion, respectively.[19] However, in the majority of scientific publications on exciton diffusion in organic semiconductors, the factor of two is omitted in Equation (2):

$$L_D = \sqrt{ZD\tau}\ . \quad (3)$$

In this case the value L_D is approximately equal to the average displacement of a particle from its initial position. To be consistent with the literature we will refer to the diffusion length that is given by the expression (3).

Amorphous and polycrystalline thin films of organic semiconductor are characterized by a significant degree of disorder, in particular when they are cast from solution. Variation of molecular conformations and size of conjugated segments (especially conjugated in polymers), inhomogeneity of intermolecular interactions, chemical defects and impurities, etc. lead to a Gaussian distribution of the HOMO-LUMO energy gaps – and excitonic energies. Förster or Dexter energy transfer facilitates exciton hopping among conjugated segments in solid organic material. Because of the inherent disorder, such a migration can be regarded as diffusion. Feron *et al.* showed that exciton hopping can be fully described in terms of random walk.[78]

Two Steps in Exciton Diffusion

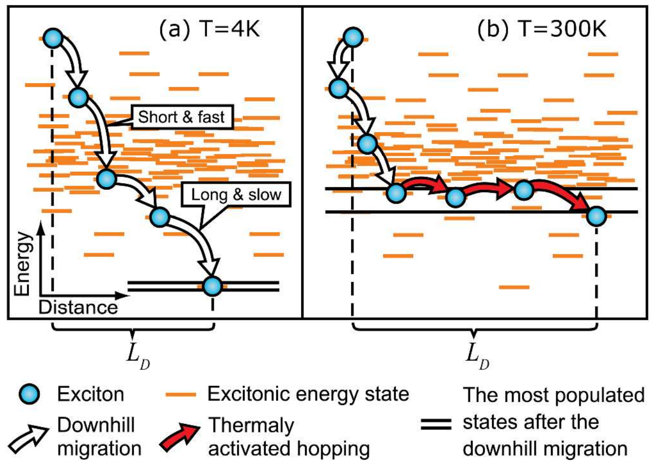

Figure 5: Exciton diffusion process at low and room temperatures. The excitonic Gaussian density of states is represented by the distribution of the excitonic energies. The exciton-phonon coupling determines the position of the energy level of the most populated states. **(a)** The downhill migration fully determines the exciton diffusion process at low temperatures. **(b)** At room temperature, the thermally activated hopping also contributes to the exciton diffusion length. (Repotted with permission from Ref. [88]. Copyright 2008 American Chemical Society)

Figure 5 schematically shows the key processes of exciton diffusion in a disordered medium, which for simplicity is considered to have a Gaussian distribution of excitonic energies with distribution width σ. Upon absorption of a photon, an exciton is created at a conjugated segment of certain energy. If conjugated segments with lower energy are available then the exciton starts a downhill migration via energy transfer toward the lower energy cites. For singlet excitons this process takes about 100 ps and can be observed by the bathochromic shift of the PL spectrum during this time.[73,74,81,89–94] The downhill migration proceeds until excitons reach a quasi-equilibrium level of the most populated states, which is located at $-\sigma^2/kT$ below the center of the Gaussian density of states (DOS).[95] The energy of this level can be measured by simply observing the position of the maximum of the PL spectrum (see **Figure 6b**).

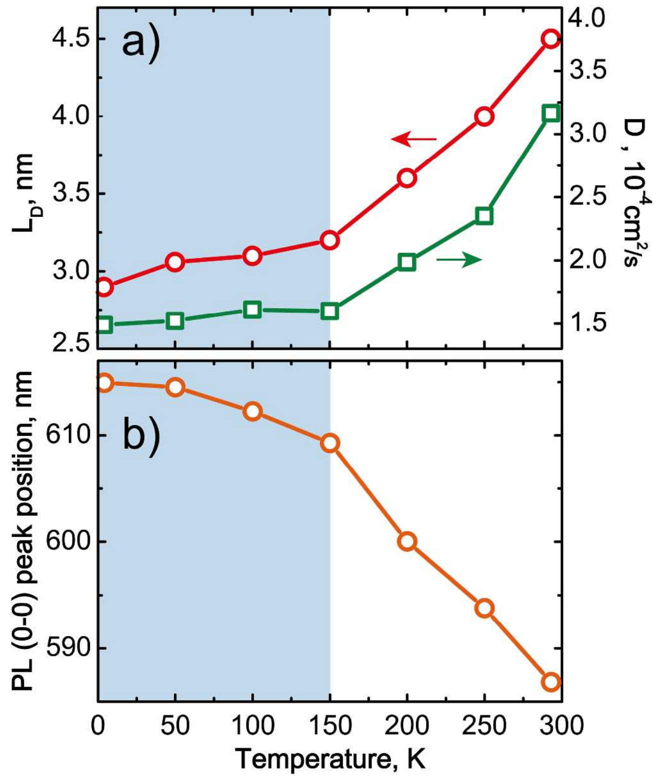

Figure 6: (a) Temperature dependence of singlet exciton diffusion length (circles) and diffusion coefficient (squares) in MDMO-PPV. **(b)** Temperature dependence of PL (0-0) position in MDMO-PPV. (Repotted with permission from Ref. [88]. Copyright 2008 American Chemical Society)

Downhill migration and thermally activated hopping determine the temperature dependence of exciton diffusion length. When poly[2-methoxy-5-(3,7-dimethyloctyloxy)-1,4-phenylene-vinylene] (MDMO-PPV) is being cooled from room temperature down to ~150 K thermally activated hopping becomes less important resulting in a decrease of diffusion length and diffusion coefficient (see **Figure 6a**). At temperatures below 150 K excitons relax down to the bottom of the DOS where the density of lower lying states is insufficient for further downhill migration. Consequently, the level of the most populated states becomes temperature independent and since in this regime there is not enough of thermal energy for activated hopping, both D and L_D become temperature independent.

The processes of downhill migration and thermally activated hopping can be observed for both singlet and triplet excitons (**Figure 5**).[68,74,75,79,81,89,90,92,93,96–107,88,108–112] Since triplet excitons undergo diffusion via short range Dexter energy transfer, the number of available hopping sites quickly becomes limited during the downhill migration. In strongly disordered systems sometimes one observes a blue shift of the maximum of phosphorescence spectrum upon cooling below 100 K.[103,104] Using theoretical modeling Beljonne, Köhler, and co-authors showed that in materials with high degree of disorder, certain thermal activation is needed for triplets to find lower energy sites, resulting in the blue shift of PL spectrum upon cooling.[81] This effect is called frustrated transport of triplet excitons and it is observed in conjugated polymers such as polyfluorene.

Strictly speaking downhill migration cannot be considered a normal diffusion that is described by Equation (1). As excitons approach the bottom of the excitonic DOS, the distance between hopping sites becomes larger, while it takes much longer time for each subsequent hop.[72,106] Under these conditions the diffusion coefficient will vary in time from larger to smaller values.[88,113] On the contrary, temperature activated hopping occurs among sites of similar energy at nearly constant site-to-site distances. Therefore, exciton migration can be regarded as a diffusion process above 150 K, where temperature activated hopping makes the dominant contribution.

Understanding Förster Energy Transfer

Since Förster energy transfer facilitates singlet exciton diffusion, we turn our attention to the factors that govern this process. The rate k_F of Förster energy transfer between donor and acceptor chromophores is given by the following expression:[114–117]

$$k_F(d) = \frac{1}{\tau_{hop}} = \frac{1}{\tau_0}\left(\frac{R_0}{d}\right)^6 , \tag{4}$$

where τ_{hop} is the hopping time between the chromophores, τ_0 is the intrinsic exciton lifetime that is not limited by diffusion limited quenching at defects, d is the distance between the chromophores, and R_o is the Förster radius:[116,117]

$$R_0^6 = \frac{9\Phi_{PL}\kappa^2}{128\pi^5 n^4}\int \lambda^4 F_D(\lambda)\sigma_A(\lambda)\, d\lambda = \frac{9\Phi_{PL}\kappa^2}{128\pi^5 n^4} J . \tag{5}$$

Here Φ_{PL} is photoluminescence quantum yield; $0 \le \kappa^2 \le 4$ is dipole-dipole orientation factor; and n is the refractive index. The integral J over wavelength λ quantifies the spectral overlap between the area-normalized PL spectrum (area under the curve must be equal to unity) of donor $F_D(\lambda)$ and the absorption spectrum of acceptor expressed in terms of absorption cross-section $\sigma_A(\lambda)$.[19,116] Then the exciton diffusion coefficient D can be estimated using Smoluchowski-Einstein theory of random walks:[118]

$$D = \frac{R^2}{6\tau_{hop}} = A\frac{1}{\tau_0}\frac{R_0^6}{6d^4}, \tag{6}$$

where A is a constant that accounts for the distribution of molecular separations d. The exciton diffusion length in a solid is then equal to:

$$L_D = \sqrt{\tau_f D} = \frac{1}{d^2\sqrt{6}}\sqrt{\frac{9\Phi_{PL}\kappa^2}{128\pi^5 n^4}\frac{\tau_f}{\tau_0}J}\ . \tag{7}$$

Here τ_f is PL lifetime in a solid film, it may be different from τ_0 due to diffusion-limited quenching at defects or even intentionally introduced quenchers in the solid medium. Equations (6) and (7) can be used to estimate exciton diffusion parameters in organic semiconductors.[114,119–122]

According to the expression (7), exciton diffusion length depends on the intermolecular spacing d, the PL quantum yield Φ_{PL}, the orientation factor κ^2, spectrally weighted refractive index n, the lifetime ratio τ_f/τ_0, and the spectral overlap J. In order to improve L_D, one has to engineer materials that optimize one or more of these parameters. The distance d can be varied in the range of 0.35 – 5 nm with the lower limit defined by the π–π stacking distance and the upper limit set by the Förster self-radius that typically values one or several *nanometers* in organic semiconductors.[64,121,123] Thus, due to the inverse quadratic dependence, L_D can be theoretically varied by two orders of magnitude by changing d. It has been shown however that optimization of PL quantum yield Φ_{PL} and spectral overlap J may have a greater impact on the diffusion length than the variation of intermolecular distance.[64] Dipole orientation factor κ^2 can be maximized when all transition dipoles are aligned, achieving a maximum value of κ^2=4. To put it into prospective, an amorphous film with randomly oriented dipoles is characterized by κ^2=0.476. Therefore, by aligning all the dipoles in the most beneficial way, L_D can be theoretically increased by ~2.9 times compared to the amorphous material.[115,124] Dipole alignment may occur naturally in single crystals; however, it is quite challenging to intentionally align them.[124] The spectral overlap J is determined by the Stokes shift, meaning that materials with smaller red-shift of emission with respect to the absorption spectrum have a potential for higher L_D. Interestingly, a higher refractive index n would lead to lower L_D, even though a high n is desirable for efficient charge separation in organic solar cells. The ratio τ_f/τ_0 depends on the amount of exciton quenching defects present in the film and approaches unity for highly pure materials. The PL quantum yield Φ_{PL} is defined as

$$\Phi_{PL} = \frac{k_r}{k_r + k_{nr}}, \tag{8}$$

where k_r is the radiative decay rate and k_{nr} is a sum of all non-radiative decay paths, excluding the diffusion-limited exciton quenching at defects. Φ_{PL} can be increased when the non-radiative decay rate k_{nr} is reduced and/or when radiative decay rate k_r is increased.

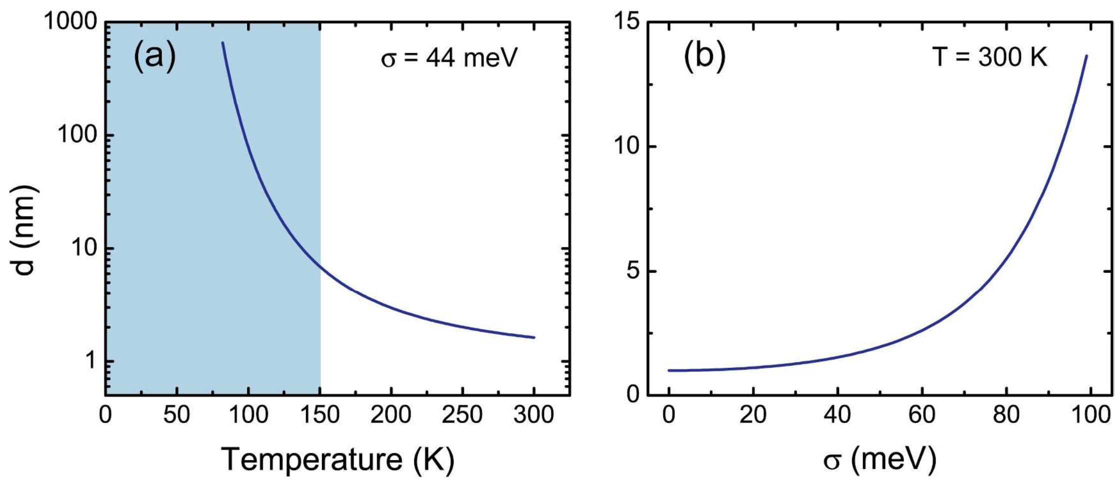

Figure 7: (a) Temperature dependence of inter-chromophore distance d at the quasi-equilibrium level for MDMO-PPV. **(b)** Dependence of d on the disorder parameter σ at room temperature. The curves were obtained using Equation (9).

It is important to note that there is no explicit temperature dependence in the expression (7). For two isolated chromophores at fixed separation d the temperature dependent parameters would be Φ_{PL} and J. At lower temperatures, the rate of non-radiative decay paths are usually reduced resulting in higher PL quantum yield Φ_{PL}. The increase of Φ_{PL} would compete with decrease of J due to reduction of inhomogeneous broadening upon cooling. Thus these effects alone would not explain the temperature dependence of exciton diffusion in solid film such as observed in MDMO-PPV (see **Figure 6**).

The temperature dependence of the exciton diffusion length is mainly determined by the intermolecular separation d between excitonic sites that take part in temperature activated hopping (see **Figure 5**). If thermal quasi-equilibrium can be reached during the exciton lifetime then the distance between chromophores at the energy level of the most populated states after downhill migration is:[95]

$$d_{eq} = \left[n_{eq} \right]^{-\frac{1}{3}} = \left[N_0 \exp\left(-\frac{\sigma^2}{2(kT)^2} \right) \right]^{-\frac{1}{3}}, \qquad (9)$$

where n_{eq} is density of excitonic states with energy at the quasi-equilibrium level, N_o is the total density of available excitonic states that is on the order of 10^{21} cm^{-3} for organic semiconductors. To illustrate the importance of the temperature dependence of d_{eq} we consider MDMO-PPV with known disorder parameter σ=*44 meV* (Ref. [88]). **Figure 7a** shows that d_{eq} increases upon reduction of the temperature and below 150 K it quickly becomes larger than the range of Förster energy transfer, *i.e.* 1-5 nm. Therefore, the transition between the two regimes of exciton diffusion occurs at this temperature (see **Figure 6a**).

Expression (9) also highlights the impact of disorder on exciton diffusion. Materials with higher disorder parameter σ show higher d_{eq} as it is presented in **Figure 7b** for room temperature. Consequently exciton diffusion is usually higher in more ordered materials. **Figure 7b** suggests that thermally activated hopping at room temperature can be only observed in materials with σ < *80 meV*, at which d_{eq} is within the range of Förster energy transfer. It is important to note that the excitonic disorder parameter

σ is usually ~2 times smaller than the disorder parameter extracted from charge transport measurements.[88,125]

In amorphous films of conjugated polymers, it is observed that exciton diffusion is isotropic.[126,127] However, in organic crystals, both singlet and triplet exciton transport appears to be highly anisotropic due to Bravais lattices with low degree of symmetry such as triclinic systems with several molecules per unit cell.[19] Anisotropy of singlet exciton diffusion is also enhanced by the strong dependence of the Förster energy transfer rate on their mutual orientation of participating chromophores.[84,115,124,128–130] Dexter energy transfer strongly relies on the spatial overlap of the wavefunctions of the excited states at neighboring molecules. Such overlaps are also highly anisotropic in organic crystals, having the highest values at π-π stacking direction.

Exciton-Exciton Annihilation

High exciton densities and diffusion processes give rise to a high probability of two excitons meeting each other during their lifetimes. Exciton-exciton annihilation occurs when the interaction between these two excitons leads to a non-radiative recombination of at least one of them.[2,131–136] For instance, annihilation of two singlet (S_1) or two triplet (T_1) excitons may result in a ground state (S_0) and a singlet exciton:

$$S_1 + S_1 \rightarrow S_0 + S_1, \tag{10}$$

$$T_1 + T_1 \rightarrow S_0 + S_1. \tag{11}$$

Other products of exciton annihilation are also possible.[137] Efficient triplet exciton annihilation (11) requires anti-parallel spins of triplet excitons due to the conservation law of angular momentum. Singlet excitons that are created as the result of triplet exciton annihilation (11) may decay radiatively. Such emission is called delayed fluorescence because it can be observed after a pulsed laser excitation at times much longer than the PL decay time.[2,26,98,99,102,131,133,134,138–153]

Exciton-exciton annihilation can be described mathematically by the following modification of the Equation (1):

$$\frac{\partial n}{\partial t} = D\nabla^2 n - \frac{n}{\tau} - \gamma n^2 + G, \tag{12}$$

$$\gamma = 4\pi R_a D; \tag{13}$$

where γ is the annihilation rate constant, R_a is the annihilation radius – the average distance between two excitons that undergo annihilation, and G is the exciton generation rate.

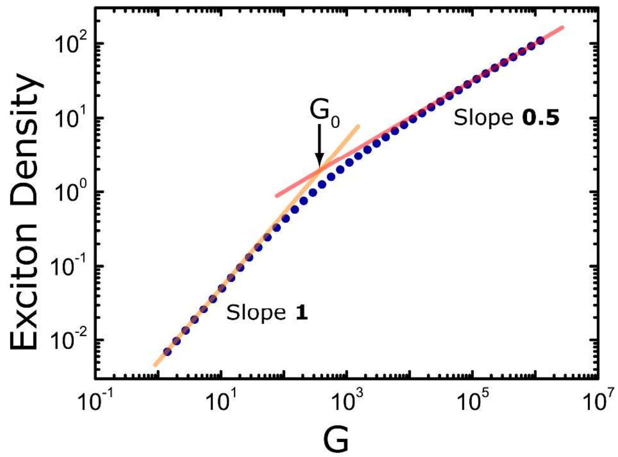

Figure 8: Simulated exciton density (circles) *versus* the exciton generation rate using Equation (15).

Under conditions of continuous and homogeneous generation $G = const$ we can set $\partial n / \partial t = 0$ and $\nabla^2 n = 0$ in Equation (12):

$$\gamma n^2 + \frac{n}{\tau} - G = 0, \tag{14}$$

leading to the steady state solution:[135]

$$n = \frac{1}{2\gamma\tau}\left(\sqrt{1 + 4\gamma\tau^2 G} - 1\right). \tag{15}$$

Figure 8 shows an example plot of Equation (15) when $4\gamma\tau^2 = 0.01$ (circles). The dependence consists of two straight lines with slopes 1 and 0.5. In a log-log graph a straight line denotes function in a form of $y = cx^\alpha$, where α is the slope of that line. Slope 1 denotes linear dependence $n \propto G$ at generation intensities smaller than a certain threshold value G_0. The square root dependence $n \propto \sqrt{G}$ at $G > G_0$ indicates the exciton-exciton annihilation. The threshold generation rate can be estimated from Equation (15):

$$G_0 \approx \frac{1}{\gamma \tau^2}. \tag{16}$$

The expression (16) shows that the exciton-exciton annihilation is a more important decay process for triplets than for singlets because of the long triplet lifetime τ. Triplet-triplet annihilation can be observed by recording the dependence of the phosphorescence intensity or the photoinduced absorption intensity (transition **7** in **Figure 2**) on the generation rate G,[102,154] or by observing delayed fluorescence – emission of singlet excitons that are a product of the process shown in expression (11).[2,26,98,99,102,131,133,134,138–153]

Diffusion Limited Exciton Quenching

Excitons can be quenched in several ways leading to the reduction of the exciton density, PL intensity, and PL decay time. Exciton quenching is a very important process in operation of devices and for studying exciton dynamics. The energy of an excited state can be trapped during the diffusion process on defects that are always present in thin films of organic semiconductors. Trapped excitons are usually quenched since the defects often do not show photoluminescence. Strong quenching has been observed in the vicinity of metal interfaces.[155] Exciton dissociation into non-radiative species such as free electrons and holes also leads to quenching. Inhomogeneous regions in amorphous films of higher molecular density, as expressed in g/cm^3 etc., show higher rates of exciton quenching.[156–159] Furthermore, exciton quenching has been also observed at grain boundaries of polycrystalline materials.[160]

Figure 4 illustrates the dissociation of an exciton at the semiconductor (electron donor) – fullerene (electron acceptor) interface. In the most common situation the LUMO of fullerenes is significantly lower than the LUMO of many organic semiconductorss.[32] Thus electron transfer to the fullerene is energetically favorable, which leads to exciton quenching. Exciton quenching due to charge transfer at the semiconductor-fullerene interface is reported to be at the time scale of 45 fs, which is much shorter than the typical exciton lifetime (~0.5 ns). Therefore, fullerenes can be considered as perfect exciton quenchers for donor semiconductors.[161]

3. Measuring Singlet Exciton Diffusion Length

The singlet exciton diffusion length is typically reported in the range of 5-20 nm in amorphous and polycrystalline organic semiconductors.[31,55,63,88,114,126,127,155,156,160,162–180] Table I summarizes exciton diffusions of various organic semiconductors and methods used to measure them. It is not entirely clear why the exciton diffusion length is so similar in such a broad selection of materials. What factors influence the exciton diffusion length? And finally how do these factors – and the exciton diffusion length itself – correlate with the performance of solar cells and LEDs? To answer these questions systematic measurements of exciton diffusion lengths are needed in materials with various chemical composition, morphology and performances in devices.[63,128,160,171] In the following we summarize the available methods and discuss the advantages and pitfalls of each technique. Lin *et al*. provided a comprehensive comparison of most of these methods by applying them to a set of small molecule compounds.[121] Chart I summarizes key features of each approach to measure singlet exciton diffusion length.

Chart I. Comparison of various methods of measuring singlet exciton diffusion length. Relative degree of preference (or ease) is presented as a number of star signs: with three stars (□□□) for most preferred and easy procedures, and one star (□) for the least preferred (or hard to do) item.

Technique	Sample Preparation	Measurement	Data Analysis	Best for

Fluorescence quenching in bi-layers	★ ~10 bi-layer films with quenching layer and varying thickness of organic semiconductor; ~10 pristine films of different thickness	★★ PL decay time or ★ PL intensity; accurate film thickness measurement; optical constants	★★★ An analytical model often can be applied	★ Amorphous smooth films. (!) Sharp and highly quenching interface is required
Fluorescence volume quenching	★★★ Only two films are required	★★★ PL decay time or ★ PL intensity; film density	★★★ Stern-Volmer analysis for monoexponential decays, or free Monte Carlo Simulation for multi-exponential PL decays	★★ Moderately polycrystalline or amorphous films

Exciton-exciton annihilation	★★★ Only one pristine film is required	★★ PL decay time under different excitation intensities, but annihilation cross-section is hard to measure	★★★ Analytical model is available	★★ Amorphous, polycrystalline, or crystalline materials with exceptional photo-stability
Microwave Conductivity	★ ~ 5-10 bi-layer films with semiconductive quenching layer (TiO_2) and varying thickness of organic semiconductor	★ Custom combination of optical and microwave measurements	★★★ An analytical model can be applied	★★ Amorphous materials with non-emissive excitons
Electro-optical measurements	★ A full device has to be prepared such as solar cell or LED	★★ Measurement of device parameters such as external quantum efficiency	★ Modeling usually has multiple fitting parameters including charge transport	★★ Amorphous or polycrystalline materials with non-emissive excitons; n-type materials

Fluorescence Quenching in Bilayers

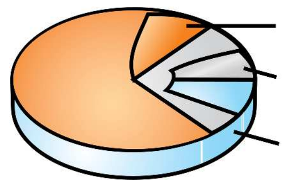

Figure 9: Bilayer structure for exciton diffusion measurement. The organic semiconductor is deposited on top of an exciton-quenching layer. (Adapted with permission from Ref. [88]. Copyright 2008 American Chemical Society)

Perhaps the most popular method to measure singlet exciton diffusion length is based on PL quenching in bilayers.[31,63,88,127,156,164,166,167,169,170,173,178,181–184] In this method one of the interfaces of a thin film is brought into contact with an exciton quenching layer (**Figure 9**). Fullerenes or TiO_2 are commonly used as "quenching wall". If the thickness of the organic layer is of the order of the exciton diffusion length, then a large fraction of the excitons will be able to reach the "quenching wall" via diffusion. Consequently, the PL decay time of such a sample will be shorter than in an isolated film. The measured PL decays are then fitted using a simple model that is based on Equation (1), yielding the exciton diffusion length. Examples of such models can be found in references [88,169,173,179].

There are advantages and disadvantages of the bilayer method. On the positive side the modeling is straightforward with the exciton diffusion length as the only fitting parameter. The thickness of the semiconductor layer can be accurately measured using atomic force microscopy or ellipsometry. On the other hand the sample preparation is quite demanding because one needs to prepare a series of an organic semiconductor with various film thicknesses. Additionally, it may be challenging to prepare semiconductor layers as thin as 5 nm that are uniform in thickness and do not form pin-holes or other defects. Furthermore, all the interfaces should be sharp[173] and ultra-flat; typically root mean square roughness of about 1 nm on the area of 100 μm^2 is required for accurate measurement. The quenching efficiency of the "quenching wall" must be carefully evaluated to get an accurate measurement.[167] The effects of optical interference[169,185] and variation of the exciton density due to optical absorption[166] must be taken into account. Often PL decay times of isolated films also depend on the layer thickness even without the introduction of any quenchers.[156,166,186] All these factors set limits to use the bilayer structure for systematic measurements of the exciton diffusion length.

If there is a significant overlap between the emission spectrum of the semiconductor and absorption spectrum of the quencher, then excitons can be quenched by a direct Förster energy transfer to the quenching molecule (see **Figure 3a**). In some cases Förster energy transfer may become a dominant exciton-quenching pathway as opposed to the electron transfer. FRET may occur between chromophores at distances of 2-3 nm that is comparable to the exciton diffusion length. Therefore, this effect must be taking into account when modeling exciton diffusion in bilayers.[31,64,114,120,169]

The problematic thickness-dependent effects can be avoided in an alternative bilayer method.[114,160,165,179,187,188] A thick film, typically of the order of micrometers, is capped either with an exciton blocking or exciton-quenching layer. This heterostructure is excited with monochromatic light at various wavelengths. Depending on the absorption cross-section at each wavelength, the exciton generation profile is modulated. By comparing the PL intensity of quenched and unquenched samples the exciton diffusion length can be extracted. The advantage of this method is that only two samples are needed for each material. However, the mathematical model is complex and this method works best when the variation of the generation profile is significant on the length scale of the exciton diffusion length. Therefore, it is most applicable for single crystals, which show extremely long exciton diffusion length.[179,187] However, Bergemann *et al.* showed that this method can be used for optically thin films as well.[189]

Fluorescence Volume Quenching

In order to overcome the shortcomings of the bi-layer method, one can apply a fluorescence volume quenching technique of measuring exciton diffusion length.[119,120,122,126,190–193] In this method, an organic semiconductor is mixed with small amounts of exciton quenching molecules, typically a fullerene derivative phenyl-C61-butyric acid methyl ester (PCBM) at blend ratios of 0.001 – 5 wt%. Then the PL decay time is measured as a function of PCBM volume fraction. As the concentration of quenchers is increased, PL decay time becomes shorter due to the diffusion-limited quenching. This happens when the average distance between quenching molecules approaches the exciton diffusion length. By carefully controlling the concentration of PCBM one can get a handle of how far excitons are able to diffuse.

In order to get an accurate measurement of the exciton diffusion length using the fluorescence volume quenching method it is important to use the correct theoretical model to fit experimental results to extract exciton diffusion coefficient, and to control the nanoscale morphology of the semiconductor-quencher blends. In the most general case, the exciton diffusion in blends can be modeled using free open source Monte Carlo simulation.[190,194] Samuel and co-workers modeled PL decays of semiconductor-quencher blends using the Smoluchowski equation.[122,123] If the material shows monoexponential PL decays, one may apply a simple Stern-Volmer analysis.[116,195–200] These modeling approaches allow extracting the exciton diffusion coefficient typically as the only fitting parameter.

For the sake of modeling, it is necessary that PCBM forms an intimate mixture with the semiconductor at various blend ratios where significant PL quenching is observed. The morphology of the semiconductor-PCBM blends can be probed by surveying a range of PCBM concentrations. If experimental data can be modeled with a single value of diffusion coefficient within a certain range of concentrations then PCBM molecules form intimate blends within this range.[190] Often, it is more likely that PCBM would form phase-separated clusters at higher concentrations. Clustering results in reduction of the interfacial area between PCBM and semiconductor as compared to the intimate mixture of the same PCBM loading, leading to a reduction of exciton quenching efficiency. As a result, phase-separated blends with PCBM clusters would yield a lower diffusion coefficient as the PCBM concentration is increased.

Exciton-Exciton Annihilation

The exciton diffusion coefficient can be estimated by measuring the efficiency of the exciton-exciton annihilation.[110,133,162,163,165,166,168,201–208] The exciton diffusion coefficient is calculated from γ, given Equation (13), which can be measured experimentally by modeling the PL decays measured at various excitation intensities of the incident light. Only one sample is needed for the measurements. However, the theoretical considerations are complex and there are two unknown parameters that are needed for the modeling, namely the annihilation radius R_a and initial exciton density n_0. It is quite difficult to set an independent experiment to measure these parameters and they are typically assumed to have a certain value. Only materials with exceptional photochemical stability can be investigated using this method because intense laser light is required to create high enough exciton density for the exciton-exciton annihilation to occur.

Microwave Conductivity

An interesting method to measure exciton diffusion lengths has been developed at Delft University.[175,209–214] Exciton quenching in semiconductor-TiO_2 bilayers has been estimated by observing enhancement in photoconductivity in the TiO_2 layer due to electron transfer from the semiconductor layer. The change in photoconductivity is estimated by measuring the change of the intensity of reflected microwave radiation upon optical excitation of the semiconductor. The microwave conductivity in TiO_2 is then modeled depending on the thickness of the organic layer. The important advantage of this method is that it is also sensitive for non-emissive excitons, such as triplets. However, this method has all the problems of the PL quenching methods in bilayers as discussed above and therefore it is also not ideal for systematic studies of exciton diffusion.

Electro-Optical Measurements

Exciton diffusion length can be estimated by modeling current-voltage (I-V) characteristics of a solar cell, of an OLED, or a similar device.[55,63,176,177,180,184,187,215–224]

The typical sample consists of at least one organic semiconductor layer and two electrodes. The theoretical model includes the electrical, optical, and exciton diffusion parts. It is a big challenge to describe the charge transport through a specific organic layer as well as to understand charge injection/extraction at the electrical contacts. The effect of metallic electrodes on the distribution of the excitation light – and generated excitons – within the device must be carefully calculated.[169,225] Exciton quenching at metallic electrodes should be also included into the model. These photocurrent measurements are the most difficult way to extract the exciton diffusion length. It is reasonable to apply this method to a semiconductor that does not show efficient photoluminescence.

4. Controlling Singlet Exciton Diffusion Length

In order to improve the device performance of organic solar cells and OLEDs, there have been multiple attempts to understand what factors limit exciton diffusion length. The common strategies to enhance singlet exciton diffusion include controlling the degree of crystallinity and optimizing Förster energy transfer. In addition, it has been also pointed out that elimination of ubiquitous exciton quenching defects may also lead to improvement of the diffusion length.[73,195,226,227] In this section, we summarize recent findings in this area of research.

Theoretical Limit of Exciton Diffusion Length

Yost *et al.* presented an interesting theoretical study, in which singlet and triplet diffusion processes were considered by purely *ab inito* means.[228] The authors examined fundamental limits of increasing exciton diffusion length and used tetracene as an example. They argue that for singlets it is difficult to increase the diffusion coefficient without decreasing the exciton lifetime. The only physical parameter that varies from material to material and influences the diffusion length is the transition dipole. The diffusion coefficient is increasing with transition dipole, while the radiative decay time is decreasing. Therefore, the singlet exciton diffusion length has its theoretical maximum of ~100 nm for tetracene. For triplets, diffusion coefficient and lifetime can be varied independently, thus there is no fundamental limit in increasing the diffusion length. Triplet excitons have long lifetime due to spin-forbidden transition to the ground state, while diffusion coefficient is mainly determined by the wavefunction overlap of the neighboring molecules.

Optimizing Exciton Diffusion

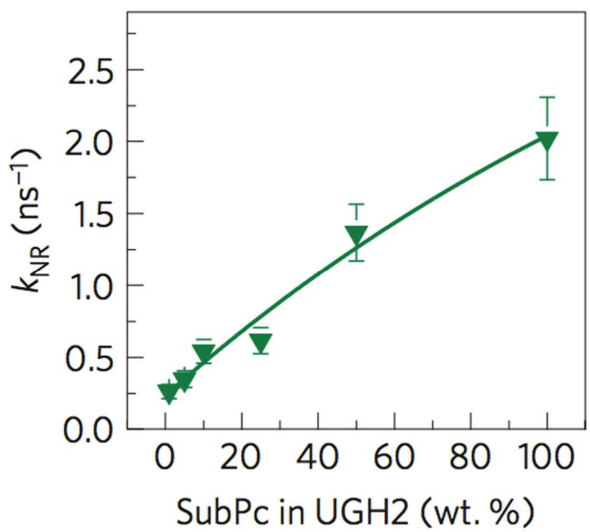

Figure 10: Dependence of non-radiative decay rate of a subphthalocyanine (SubPc) in blends with high bandgap matrix UGH2. (Reprinted by permission from Macmillan Publishers Ltd: Nature Materials Ref. [64], copyright 2013)

Optimization of exciton diffusion length relies on the ability to fine tuphthalocyaninene parameters in the expression (4). A nice illustration of reduction of the non-radiative decay rate k_{nr} was presented by Menke *et al.*[64,229] Exciton diffusion length has been increased from 10.7 to 15.3 nm in subphthalocyanine derivative by blending the subphthalocyanine within a high band gap matrix 1,4-phenylenebis(triphenylsilane) (UGH2) (see **Figure 10**). Intermolecular interactions between subphthalocyanine molecules are suppressed in such blends resulting in reduction of self-quenching. The performance of the bi-layer solar cell is increased by 30% when utilizing this approach. Raisys *et al.* made systematic chemical modifications to a series of nine triphenylamine (TPA)-cored derivatives by incorporation of phenylethenyl side-arms. Exciton diffusion length in these compounds shows improvement from 1 to 7 nm upon increase of the number of side-arms. Such an increase is attributed to the increase of the spectral overlap J by means of reduction of the Stokes-shift and enhancement of the extinction coefficient in compounds containing a larger number of the side-arms.

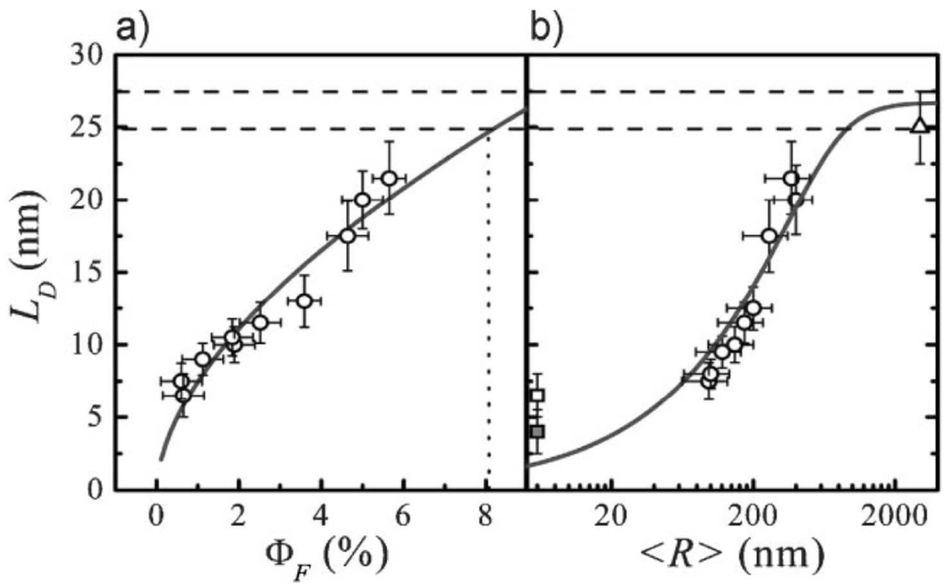

Figure 11: Dependence of exciton diffusion length on **(a)** PL quantum yield and **(b)** mean crystal diameter in polycrystalline (hollow circles) films of PTCDA. Amorphous film is presented as squares. Dashed lines represent the single-crystalline limit. (Reprinted with permission from Ref. [160]. Copyright 2010 WILEY-VCH Verlag GmbH & Co. KGaA, Weinheim)

In many cases materials with higher degree of order or crystallinity show higher singlet diffusion length. Lunt *et al.* used spectrally resolved PL quenching to measure singlet exciton diffusion in 3,4,9,10-perylenetetracarboxylic dianhydride (PTCDA).[160] **Figure 11b** shows that exciton diffusion length is increased from 6 to 20 nm as the average diameter of crystalline domains is enhanced from 100 to 400 nm. Such an increase is attributed to the reduction of non-radiative losses at grain boundaries, which is also reflected in correlation of PL quantum yield and exciton diffusion length (see **Figure 11a**). Yang *et al.* studied exciton diffusion in Zn- phthalocyanine films with different degree of crystallinity and observed an increase of L_D from 9 to 16 nm.[230] Lin *at al*. systematically measured the exciton diffusion length in three small molecule organic semiconductors based on diketopyrrolopyrrole (DPP) with incremental chemical modifications and found that material with highest degree of crystallinity showed an exciton diffusion length of 13 nm, while the least crystalline compound resulted in L_D of 9 nm.[121] Rim et al. showed that the exciton diffusion length is longer in more ordered *trans*-isomer (5 nm) as compared to the disordered *cis*-isomer (2.6 nm) in a perylene derivative.[184] Sim *et al*. measured the exciton diffusion length in poly(3-hexylthiophene) (P3HT) using a method of spectrally-resolved PL quenching in bi-layers as a function of thermal annealing.[231] They found that the exciton diffusion length is increased from 3.3 to 7 nm with increasing the annealing temperature, which leads to enhancement of the crystalline ordering. The factors, which directly influenced the exciton diffusion length include improvement of the spectral overlap J between emission and absorption of more ordered film, as well as reduction of energetic disorder resulting in more efficient exciton diffusion. Exciton diffusion length in a squaraine derivative has been increased from 1.6 to 5 nm upon thermal annealing.[188] Exciton diffusion lengths above 20 nm have been only reported in single crystals or in polycrystalline films with large grains due to low degree of disorder yielding short interchromophore distances d_{eq} at the quasi-equilibrium level, see Equation (9) and **Figure 7b**.[85,160,179,203,216,223,232,233]

On the other hand, thermal annealing can also lead to steep reduction of exciton diffusion length. It has been shown that despite enhanced crystalline ordering, the exciton diffusion length was reduced from 9 to 3 nm in a DPP derivative upon heating at 80 °C for 10 minutes.[234] Such a reduction in diffusion length is related to the quenching at grain boundaries that appear in the film upon amorphous-polycrystalline transition. Similar effect has been observed in poly[3,4-dihexyl thiophene-2,2′:5,6′-benzo[1,2-b:4,5-b′]dithiophene] (PDHBDT) by Ko *et al*.[235] In PDHBDT exciton diffusion lengths decreased upon thermal annealing from 12.5 to 6 nm. And finally is has been also shown that processing organic semiconductors with high boiling point additive can result in reduction of exciton diffusion length despite apparent increase in the degree of crystallinity.[65] Films that were processed with the additive have additional excitonic traps, which are responsible for reduction of the diffusion length.

An interesting approach to modulation of exciton diffusion length was presented by Ortiz *et al.*[236] They showed that the addition of heavy atom substituent (iodine) to a porphyrin molecule yields in systematic reduction of exciton diffusion length from 15 to 4 nm. This effect is linked to enhanced intersystem crossing of singlet excitons to triplet manifold resulting in reduction of singlet lifetime and thus L_D.

Trap-Limited Exciton Transport

In solid films of organic semiconductors, excitons diffuse and may encounter impurities and morphological and chemical defects resulting in exciton quenching. These trap states may limit L_D if the average distance between traps becomes similar to L_o, the exciton diffusion length of a defect-free material. The impact of trap-limited quenching on L_D can be quantified by the lifetime ratio $\tau_{\square}/\tau_0$ that enters Equation (7):

$$L_D = L_0 \sqrt{\frac{\tau_f}{\tau_0}} \,. \tag{17}$$

The intrinsic exciton lifetime τ_0 is usually estimated from PL measurement in a dilute solution. However, this approach of determining τ_0 may be invalid in case of strong intermolecular interactions. The density of excitonic traps c_o can be estimated using Stern-Volmer analysis:[195]

$$c_0 = \frac{1}{4\pi D}\left(\frac{1}{\tau_f} - \frac{1}{\tau_0}\right) . \tag{18}$$

Using the obtained expression and a Monte-Carlo simulation we showed that exciton diffusion length is indeed limited by the defect states in a series of common amorphous organic semiconductors[195] and that the density of exciton traps is within the range of 10^{17}-10^{18} cm^{-3} in eleven studied materials. The average distance between these traps then determines the exciton diffusion length: $L_D = \left(2\sqrt[3]{c_0}\right)^{-1}$ resulting in values of L_D in the range of 5-10 nm (see Table I).

Interestingly, the obtained density of excitonic traps is nearly equal to the density of electron traps that are observed in common organic semiconductors.[227] Since exciton quenching and electron trapping are essentially the same process of electron transfer to the trap site, it is suggested that these are the same species. Liang *et al*. made an observation that leads to a similar conclusion by studding n-type doping of P3HT with cobaltocene.[226] They saw a simultaneous increase in conductivity and PL lifetime upon increase of dopant loading. The authors related this effect to the filling the trap states with the help of electron donating ability of cobaltocene. The maximum of conductivity and PL lifetime was achieved at dopant concentration of 1.2×10^{18} cm^{-3} that corresponds to the density of exciton quenchers that was found by our work.

Athanasopoulos *et al*. presented a theoretical prediction of trap-limited exciton transport.[73] They developed a comprehensive Monte Carlo simulation of exciton diffusion with detailed exciton hopping model, in which transfer rates were calculated for 50 nearest neighbors during each hop. As an example experimental data of a polyfluorene derivative have been used. Most of the input parameters were deduced from absorption and emission spectra. The resulting L_D of ~60 nm is similar to the values typically obtained from single crystals. However, inclusion of excitonic traps enabled them to explain the smaller measured value of ~10 nm.

5. Triplet Exciton Diffusion

Triplet excitons are expected to have longer diffusion length than singlets due to their much longer lifetime, see Equation (3) and Table II. However, values as short as 10-20 nm have been reported recently, similar to the singlet exciton diffusion length.[114,237–243] On the other hand, there are plenty of publications with triplet diffusion length of more than 100 nm.[5,9,44,187,244–246] Moreover, different values in the range of 10-250 nm have been published for the same materials.[53,143,238,239,244] Such a controversy probably stems from the use of different methods to measure triplet exciton diffusion. Most available techniques are complex and it is hard to control the relevant processes that influence the exciton diffusion length such as triplet-triplet annihilation. Simple PL quenching techniques can only be applied to phosphorescent materials.[114,247] Here we summarize notable methods used to measure the triplet exciton diffusion length (see Chart II).

Chart II. Comparison of various methods of measuring triplet exciton diffusion length. Relative degree of preference (or ease) is presented as a number of star signs: with three stars (□□□) for most preferred and easy procedures, and one star (□) for the least preferred (or hard to do) item.

Technique	**Sample Preparation**	**Measurement**	**Data Analysis**	**Best for**
Direct observation delayed luminescence spread	★★ Large homogeneous sample or single crystal	★★ microscope imaging or usage of secondary structures	★★★ An analytical model is available	★ Single crystals with large triplet diffusion length
Measurement in LED configuration	★ Multiple working multilayer OLED devices	★★ PL intensity vs thickness of active layer	★ Modeling is complex with multiple fitting parameters	★ Amorphous smooth materials with good charge transport properties

Photocurrent and microwave conductivity	★ Bi-layers, which are included in a working solar or used for microwave conductivity	★ Measure device parameters such as external quantum efficiency or use custom combination of optics and microwaves. Hard to distinguish between singlet and triplet excitons	★★ Modeling is sophisticated, but an analytical model sometimes can be used	★★ Amorphous smooth materials, single crystals
Remote phosphorescent sensing	★★ ~10 multilayer films, typically vacuum deposited	★★ PL intensity or PL lifetime	★★ Depending on sample structure modeling can be very simple or quite complex	★★ Amorphous materials

Modeling of absorption transients	★★★ Only one pristine sample is required	★ Requires sophisticated equipment with multiple laser beams, extra care must be given to measure at low laser intensities	★★ Analytical models usually have multiple fitting parameters	★★★ Amorphous, polycrystalline, and crystalline materials.

Direct Observation Delayed Luminescence Spread

Perhaps one of the oldest methods of measuring triplet exciton diffusion is based on detection of the spatial spread of delayed fluorescence in single crystals.[5,131,151,248,249] The main idea of this method is based on localization of triplet generation region to a small area with linear dimensions smaller or similar to the diffusion length. Triplet excitons diffuse outside from the generation area and undergo triplet-triplet annihilation. The resulting delayed fluorescence is then detected as a function of time and/or intensity of generation. Then the data is fitted to the diffusion equation with the annihilation term being dependent on in diffusion length. In this way exciton diffusion lengths of ~1-10 μm were extracted in antracene,[82,248] tetracene,[246] and rubrene[5] crystals. This method can be only applied for systems with triplet diffusion length in the order of a micrometer.

Measurements in LED Configuration

A specially designed multilayer LED can be used to measure triplet exciton diffusion.[44,53,140,237–239,250–252] In this structure, the charge recombination region is spatially confined within a thin interfacial region between electron and hole transporting layers. A phosphorescent dopant is deployed in one of the transporting layers at certain distance L from the exciton generation region. The materials are selected such that triplet energy transfer from the host semiconductor to the dopant is favorable. Then the intensity of phosphorescent emission of the dopant molecules is correlated to the triplet density of the host material in the vicinity of the dopant layer, *i.e.* at distance L from the charge recombination region. The profile of triplet exciton density within the semiconductor layer is measured by recording the dependence of phosphorescence intensity of the dopant molecules *versus* distance L. This profile is theoretically modeled to extract the exciton diffusion length.

The emission intensity of the phosphorescent dopant is strongly affected by the outcoupling efficiency that must be carefully calculated and included into the model. In a working LED, there is a significant amount of polarons that are efficient quenchers of triplet excitons. However, polaron-triplet interactions have been always neglected in the LED-based methods.[253] The thickness and position of the recombination region depends on the total electrical current that flows through the device. These effects set certain limits on the value of the working current. It is difficult to evaluate the effect of triplet-triplet annihilation in this method. Due to many complications and uncertainties in the LED methods, it is not surprising that very different values of the triplet diffusion length have been extracted in the same materials.

Photocurrent and Microwave Conductivity

Similar to singles, triplet exciton diffusion length can be also measured in using previously described methods such as the photocurrent modeling[6,217,240,241,244,254–257] and the microwave conductivity measurements.[209,242] In these methods it is important to distinguish contributions of triplet vs. singlet excitons to photocurrent or microwave conductivity leading to an additional complication. Usually the effect of triplet-triplet annihilation is not taken into account when applying these methods. Values of triplet exciton diffusion lengths of 10-250 nm have been reported in several materials.

Remote Phosphorescent Sensing

Triplet exciton diffusion can be directly probed in a bilayer structure comprising a pure organic semiconductor layer and a layer that is heavily doped with phosphorescent molecules.[44,143] Triplet excitons are created by intersystem crossing in the semiconductor, followed by their diffusion toward the doped layer, where their energy is transferred to the dopants and detected as phosphorescent emission. The phosphorescence decay and delayed fluorescence are then modeled using the diffusion equation, leading to the exciton diffusion length. The model used requires four fitting parameters including the exciton diffusion length, triplet-triplet annihilation rate, transfer rate from host material to the phosphorescent dopant and the initial triplet density. In *4,4′*-bis(N-carbazolyl)biphenyl (CBP) the resulting exciton diffusion length was estimated to be 25 nm when triplet-triplet annihilation is efficient and 140 nm when the annihilation is absent.[143] Disadvantages of this method are the large number of fitting parameters and the complex theoretical model.

Triplet diffusion length can be measured directly in a three-layer structures consisting of a triplet injecting layer, an organic semiconductor, and a triplet detecting layer.[258] The triplet injector is a phosphorescent material with triplet energy higher than the triplet of semiconductor. Thus optically excited triplet excitons are transferred from the injector layer to the organic semiconductor. The injected triples then diffuse through the thickness L of organic semiconductors and can be detected by the phosphorescent triplet detector. In order to achieve efficient triplet detection, detector must have its triplet energy lower than semiconductor's triplet. By varying the thickness L, it is possible to accurately measure triplet diffusion length. In this way triplet exciton diffusion length of 90 nm was extracted in *N,N'*-di-[(1-naphthyl)-*N,N'*-diphenyl]-*1,1'*-biphenyl)-*4,4'*-diamine (NPD).

Phosphorescent Quenching

The fluorescence quenching methods of measuring exciton diffusion length can be also applied for materials that show efficient radiative decay of triplet excitons (phosphorescence).[114,247,254] Typically these materials show short triplet diffusion length similar to that of singlets. For instance, Hsu et al. studied triplet exciton diffusion in a Pt-coordinated polymer that was blended with small amounts of fullerenes.[200] Exciton diffusion length of 22 nm is extracted by modeling phosphorescence decays of these blends with Stern-Volmer equation. It is important to note, that triplet excitons can be also transported via Förster energy transfer in some metal-coordinated compounds that show high phosphorescence yields.[33–38]

Modeling of Absorption Transients

Transient absorption can be used to study in detail the dynamics of excited states in organic semiconductors.[9,206,245,259–261] Absorption spectrum of conjugated molecules in a triplet excited state usually differs from the ground state absorption. Then by tracking the time evolution of this difference in absorption, it is possible to extract triplet diffusion parameters. Using this approach Tamai *et al.* measured triplet diffusion length in polyfluorene based polymers yielding L_D of 40-50 nm. They modeled time evolution of triplet population under conditions of triplet-triplet annihilation.[259] Poletayev *et al.* estimated triplet diffusion length of 40-80 nm in thin films and 300-800 nm in crystals of pentacene.[9] Extremely long triplet diffusion length of 2-4 µm has been reported in a ladder-type conjugated polymer using detection of triplet excitons with photoinduced absorption in polymer-fullerene blends.[245]

6. Conclusions and Outlook

Exciton diffusion in organic semiconductors has been studied in the past few decades. A number of experimental techniques have been established to measure the diffusion length resulting in over a hundred values of L_D published to date. Organic crystals show a large spread of L_D ranging from 10 to 100 *nanometers* for singlets and up to several *micrometers* for triplet excitons. The majority of amorphous materials show singlet exciton diffusion length of 5-10 nm despite large variability in chemical structure. It has been suggested that singlet exciton diffusion length is limited by excitonic traps, which are present in every solution-processed organic semiconductor.

However, the nature of these traps still has to be identified in order to reduce or eliminate their impact on exciton diffusion.

The inherent disorder present in organic semiconductors to large extend determines physical processes related to exciton diffusion. At room temperature exciton diffusion is thermally activated, while below ~150 K the diffusion has dispersive character and is determined by the downhill migration of excitons within the inhomogeneously broadened excitonic density of states.

Controlling exciton diffusion length remains an interesting topic of research. Only a handful of reports showed examples of enhancement of exciton diffusion length by engineering the Förster energy transfer rate or by tweaking the chemical structure of the organic semiconductor. For light harvesting applications it is interesting to design unidirectional exciton transport by means of self-assembly.

Triplet exciton diffusion has recently reclaimed spotlight in a view of development of singlet fission solar cells. In these devices, photoinduced singlet excitons undergo a fission process resulting in two triplets. In this way it is possible to create two pairs of charges for each absorbed photon with a potential of external quantum efficiency of 200%. If successful, fission solar cells may overcome the Shockley-Queisser limit of the maximum solar cell efficiency. Triplet exciton diffusion is an important process for charge generation in the fission solar cells and thus has to be studied in more detail. Moreover, singlet fission is competing with a reverse process of triplet-triplet annihilation, also known as triplet fusion. It desirable to find ways of disabling the triplet-triplet annihilation, which is diffusion limited process.

One of the bottlenecks for the realization of electrically pumped lasers using organic semiconductors is a roll-off efficiency when driving an OLED with large current. This parasitic effect is associated with exciton quenching when interacting with injected charges. Exciton-polaron annihilation is an interesting phenomenon, which has not yet been studied in detail. Physical parameters that govern such annihilation such as annihilation cross-section have to be measured experimentally. In this respect is it is interesting to study exciton diffusion in doped organic semiconductors.

Finally there are new emerging types of materials, in which exciton diffusion has not yet been studied. These materials include TADF compounds and conjugated polyelectrolytes. In addition, more data is needed on n-type organic semiconductors, as most of the measurements of exciton diffusion length were performed on p-type materials. To achieve this, one needs to find new efficient exciton quenchers for n-type organic semiconductors.

Table I. Measured values of singlet exciton diffusion length and diffusion coefficient (❖ polycrystalline, **O** amorphous, α thermally annealed, ▯ temperature dependence measured).

Material*	**1D L_D (nm)**	**D (cm^2s^{-1})**	**Method**	**Comment**	**Reference**
$(C_{12}OCH_2)_8PcH_2$	10 - 20		PL quenching	**O**	262
1-NPSQ	2.9		spectrally resolved PL quenching	**O**	189
4P-NPD	4		LED remote sensing	**O**	222
6T	60		PL quenching in bi-layers	❖▯	186
Alq3	3 - 25	$(3 - 2000)\times10^{-6}$	exciton-exciton annihilation; PL quenching; photocurrent	**O**▯	110,170,176, 181,263,264
ASSQ	11		spectrally resolved PL quenching	**O**	189

BEH-PPV	6.5	$2{\times}10^{-3}$	PL quenching in bi-layers	○	171
BP	15		photocurrent	❖	218
C–PCPDTBT	6		PL quenching in blends	○	190
C_{60}	5 - 40		photocurrent, microwave conductivity	○	55,210,215
$C_6PT_1C_6$-DPP	12.9	$9.4{\times}10^{-4}$	various techniques	❖	121
C_6PT_2-DPP	2 - 5	(0.3 - 1.1) $\times10^{-4}$	PL quenching in blends	○ α	234
$C_6PT_2C_6$-DPP	9.2	$3.9{\times}10^{-4}$	various techniques	○	121
CoPc	1.4		photocurrent	○	63
CPB	16.8		PL quenching in bi-layers		114
CuPB	2		photocurrent	❖	218
CuPc	5 - 15, and 68		photocurrent	❖	55,63,219, 265, and 177
Dendrimers	8 - 17	(1.8 - 4.3) $\times10^{-3}$	PL quenching in bi-layers	○	183
DIP	16 - 100	$5{\times}10^{-3}$	PL quenching in bi-layers, photocurrent	❖○□	114,223,233
DPASQ	10.7		spectrally resolved PL quenching	○	189
$DTS(FBTTh_2)_2$ aka T1	3 - 7	$(3 - 5){\times}10^{-4}$	PL quenching in blends	○ α □	65,195
$EHPT_2C_6$-DPP	7.4	$4{\times}10^{-4}$	various techniques	○	121
F_{12}TBT	11		PL quenching in bi-layers	○	182

F8BT	8 - 12	5.3×10^{-4}	PL quenching in blends, and bi-layers	○	182,195
F8T2	8		PL quenching in bi-layers	○	182
FePc	1		photocurrent	○	63
H_2Pc	6.5 - 11.9		photocurrent	○	63,219,265
H_2TOPP	9.6		microwave conductivity	○ α	209
LPPP	14		PL quenching in bi-layers	❖	127
MDMO-PPV	4.5 - 6	3.2×10^{-4}	PL quenching in bi-layers	○▯	88,156,169
MEH-PPV	4 - 8	$(0.2 - 3.0)\times10^{-3}$	PL quenching in bi-layers and blends, exciton-exciton annihilation	○▯	123,168,171, 195,266
NiPc	9.1		photocurrent	○	63
NPD	5.1		PL quenching in bi-layers	○	114
NRS-PPV	3 - 6	3×10^{-4}	PL quenching in bi-layers and blends	○	172,173,195
Oligomers of fluorene		7×10^{-3}	quenching by covalently attached fullerenes	○	130
P3HT	3 - 13; 20; and 27	$(0.2 - 2)\times10^{-3}$	various PL quenching, microwave conductivity, annihilation	❖○ α	162,166,167,174,175, 182,190,195, 231,267,268; 201; and 163

PBI (J-aggregate)	96	1.3×10^{-2}	transient absorption	❖	203
PBTTT	5 - 10		photocurrent	○ α	221
$PC_{71}BM$	3	3.6×10^{-4}	PL quenching in blends	○	122
PCBM	5		exciton-exciton annihilation	○	165
PCDTBT	2 - 3	1×10^{-4}	PL quenching	○	123
PDHBDT	6 - 13		PL quenching in bi-layers	○ α	235
PEOPT	5 - 8	4.5×10^{-4}	photocurrent, PL quenching in bi-layers	○	178,215
PF12TBT	11	9.8×10^{-4}	PL quenching in bi-layers	○	269
PFBT nanoparticles	12		PL quenching	○	191
pFNI	34	2.9×10^{-2}	PL quenching in dilute solutions	○	270
PPEI	2500		PL quenching in bi-layers	❖	179
PPV	5 - 12	8×10^{-4}	PL quenching in bi-layers, photocurrent	○	164,177,180
PTCBI	3 - 5		PL quenching, photocurrent	❖	55,184
PTCDA	7 - 25; and 86 - 225	3×10^{-4}	PL quenching, annihilation, photocurrent	❖ α ▯	114,160,189,206 ; and 216
$QQT(CN)_4$	4 - 5		annihilation	❖	202
Si–PCPDTBT	6		PL quenching in blends	❖	190
SnPc	18.5		photocurrent	○	219

squarine	1.6 - 5		spectrally resolved PL quenching	❖ α	188
SubPc	8 - 16		PL quenching	○	31,64,114, 189
T2	4.3	1.2×10^{-4}	PL quenching in blends	○	195
TBCM3PP	9.4	7.9×10^{-5}	PL quenching in blends	○	236
TCM3IPP	4.4	7.3×10^{-5}	PL quenching in blends	○	236
TCM4PP	15	1.8×10^{-4}	PL quenching in blends	○	236
TEPP	7.5	7×10^{-4}	microwave conductivity	○	211
TFB	9		PL quenching in blends	○	192
TnBuPP	13	1.4×10^{-3}	microwave conductivity	○	212
TPA-cored materials	1 - 6		PL quenching in blends	○	119
TPD	17	1.5×10^{-3}	photocurrent	○	176
TPP	0.7	2×10^{-5}	microwave conductivity	○	211
ZnBuP	3	1×10^{-3}	microwave conductivity	○	214
ZnOP	15	1.4×10^{-2}	microwave conductivity	○	214
ZnPc	9 - 30		photocurrent, PL quenching	❖○	63,224,230
ZnTOPP	7 - 9		photocurrent, PL quenching	○	224,271

* 2,3,9,10,16,17,23,24-octa-n-dodecyloxymethylene phthalocyanine (**$(C_{12}OCH_2)_8PcH_2$**), 2-[4-(N-phenyl-N-1-naphthylamino)-2,6-dihydroxyphenyl]-4-[(4-(N-phenyl-N-1-naphthyliminio)-2,6-dihydroxyphenyl)-2,5-dien-1-ylidene]-3-oxocyclobut-1-en-1-olate (**1-NPSQ**), N,N′-di-1-naphthalenyl-N,N′-diphenyl-[1,1′:4′,1′′:4′′,1′′′-quaterphenyl]-4,4′′′-diamine (**4P-NPD**), sexithiophene (**6T**), tris(8-

hydroxyquinoline) aluminum (**Alq3**), 2-[4-(N,N-diisobutylamino)-2,6-dihydroxyphenyl]- 4-(4-diphenyliminio)-2,5-dien-1-ylidene}-3-oxocyclobut-1-en-1-olate (**ASSQ**), poly[2 5-bis(2-ethylhexyloxy)-1,4-phenylene vinylene] (**BEH-PPV**), tetrabenzoporphyrin (**BP**), poly[2,6-(4,4-bis-(2-ethylhexyl)-4H-cyclopenta[2,1-b; 3,4-b0]dithiophene)-alt-4,7-(2,1,3-benzothiadi-azole)] (**C–PCPDTBT**), fullerene (**C_{60}**), 2,5-dihexyl-3,6-bis[4-(5-hexylthiophene-2-yl)phenyl]- pyrrolo[3,4-c]-pyrrole-1,4-dione (**$C_6PT_1C_6$-DPP**), 2,5-dihexyl-3,6-bis[4-(2,20-bithiophene-5-yl)- phenyl]pyrrolo[3,4-c]pyrrole-1,4-dione (**C_6PT_2-DPP**), 2,5-dihexyl-3,6-bis[4-(5-hexyl-2,2′-bithiophene-5 yl)-phenyl]pyrrolo[3,4-c]-pyrrole-1,4-dione (**$C_6PT_2C_6$-DPP**), Co-phthalocyanine (CoPc), 4'-bis(9-carbazolyl)-2,2'-biphenyl (**CPB**), copper tetrabenzoporphyrin (**CuPB**), copper phthalocyanine (**CuPc**), 4 conjugated dendrimers (**dendrimers**), diindenoperylene (**DIP**), 2-[4-(N,N-diphenylamino)-2,6-dihydroxyphenyl]-4-(4-diphenyliminio)-2,5-dien-1-ylidene}-3 oxocyclobut-1-en-1-olate (**DPASQ**), 7,7′-(4,4-bis(2-ethylhexyl)-4H-silolo[3,2-b:4,5-b′]dithiophene-2,6-diyl)bis(6-fluoro-4-(5′-hexyl-[2,2′-bithiophen]-5-yl)benzo[c][1,2,5]thiadiazole) (**$DTS(FBTTh_2)_2$** aka **T1**), 2,5-dihexyl-3,6-bis[4-(5-hexyl-2,2′-bithiophene-5-yl)- phenyl]pyrrolo[3,4-c]-pyrrole-1,4-dione (**$EHPT_2C_6$-DPP**), copolymer of 9,9-didodecylfluorene and 4,7-di(thiophen-2-yl)benzo[1,2,5]- thiadiazole (**F12TBT**), poly(9,9-dioctylfluorene-alt-benzothiadiazole) (**F8BT**), Poly[(9,9-dioctylfluorenyl-2,7-diyl)-alt-bithiophene] (**F8T2**), Fe-phthalocyanine (**FePc**), H_2-phthalocyanine (**H_2Pc**), 5,10,15,20-tetrakis(4-n-octylphenyl) porphyrin (**H_2TOPP**), ladder-type poly(p-phenylene) (**LPPP**), poly[2-methoxy,5-(3,7-dimethyloctyloxy)]-1,4-phenylenevinylene (**MDMO-PPV**), poly[2-methoxy,5-(2'-ethyl-hexoxy)-p-phenylene vinylene] (**MEH-PPV**), Ni-phthalocyanine (**NiPc**), N,N'-diphenyl-N,N'-bis(1-naphthyl)-1,1' biphenyl-4, 4'' diamine (**NPD**), random copolymer of poly(2-methoxy-5-(3′,7′-dimethyloctyloxy)-p-phen- ylene vinylene) and poly[4′-(3,7-dimethyloctyloxy)-1,1′-biphen- ylene-2,5-vinylene] (**NRS-PPV**), poly(3-hexyl-thiophene) (**P3HT**), N,N0-di[N-(2-aminoethyl)-3,4, 5-tris(dodecyloxy)benzamide]-1,6,7,12-tetra(4-tert-butylphenoxy)- perylene-3,4:9,10-tetracarboxylic acid bisimide (**PBI**), poly(2,5-bis(3-hexadecylthiophen-2-yl)thieno[3,2-b]thiophene) (**PBTTT**), [6,6]-phenyl-C_{71}-butyric acid methyl ester (**$PC_{71}BM$**), {6}-1-[3-(methoxycarbonyl)propyl]-{6}-1-phenyl[6,6]-C_{61} (**PCBM**), poly[[9- (1-octylnonyl)-9H-carbazole-2,7-diyl]-2,5-thiophenediyl-2,1,3- benzothiadiazole-4,7-diyl-2,5-thiophenediyl] (**PCDTBT**), poly[3,4-dihexyl thiophene-2,2′:5,6′-benzo[1,2-b:4,5-b′]dithiophene] (**PDHBDT**), pentacene (pentacene), poly(3-(4'-(1'',4'',7''-trioxaoctyl)phenyl) thiophene) (**PEOPT**), poly[2,7-(9,9-didodecylfluorene)-alt-5,5-(4′,7′-bis(2-thienyl)-2′,1′,3′-benzothiadiazole)] (**PF12TBT**), poly(9,9-dioctylfluorene-2,7-diyl-co-benzothiadiazole) (**PFBT**), polyfluorenes with naphthylimide end groups (**pFNI**), perylene bis(phenethylimide) (**PPEI**), poly(p-phenylenevinylene) (**PPV**), 3,4,9,10-perylenetetracarboxylic bis-benzimidazole (**PTCBI**), 3,4,9,10- perylenetetracarboxylic bis-benzimidazole (**PTCBI**), 3,4,9,10-perylenetetracarboxylic dianhydride (**PTCDA**), quinoidal quaterthiophene (**$QQT(CN)_4$**), poly[(4,40 -bis(2-ethylhexyl)dithieno[3,2-b:20 ,30 -d]silole)- 2,6-diyl-alt-(2,1,3-benzothiadiazole)-4,7-diyl] (**Si–PCPDTBT**), Sn-phthalocyanine (**SnPc**), subphthalocyanine halide (SubPc), 7,7′-(4,4-bis(2-ethylhexyl)-4H-silolo[3,2-b:4,5-b′]dithiophene-2,6-diyl)bis(5-fluoro-4-(5′-hexyl-[2,2′-bithiophen]-5-yl)benzo[c][1,2,5]thiadiazole) (**T2**), 5-(4-Bromophenyl)-10,15,20-tris(4-carbomethoxyphenyl)- porphyrin (**TBCM3PP**), 5,10,15-Tris(4-carboxymethoxyphenyl)-20-(iodophenyl)- porphyrin (**TCM3IPP**), 5,10,15,20-Tetrakis(4-carbomethoxyphenyl)porphyrin (**TCM4PP**), meso-tetra(4-ethylphenyl)porphyrin (**TEPP**), [9,9-dioctylfluorene-co-N-(4-butylphenyl)-diphe- nylamine] (**TFB**), meso-tetra(4-n-butylphenyl)porphyrin (**TnBuPP**), triphenylamine-cored compounds (**TPA-cored materials**), N, N'-diphenyl-N,N'-bis(3-methyl-phenyl)-1,1'biphenyl-4,4'diamine (**TPD**), meso-tetraphenylporphyrin (**TPP**), {meso-tetrakis[3,5-bis(tert-butyl)phenyl]porphyrinato}zinc(II) (**ZnBuP**), {meso-tetrakis[3,5-bis(methoxymethyl)-phenyl]porphyrinato}zinc(II) (**ZnOP**), zinc phthalocyanine (**ZnPc**), zinctetra-(octylphenyl)-porphyrin (**ZnTOPP**).

Table II. Measured parameters of triplet exciton diffusion. (☐ single crystal, ❖ polycrystalline, **O** amorphous, ▯ temperature dependence measured).

Material*	**1D L_D (nm)**	**D (cm^2s^{-1})**	**Method**	**Comment**	**Reference**
$(C_{12}OCH_8)_8PcZn$	23	9×10^{-8}	annihilation	❖	208
$(C_{18}OCH_2)PcH_2$	64	1.6×10^{-5}	annihilation	❖	207
1,4-dibromonaphtalane	8400	3.5×10^{-4}	annihilation, delayed PL	☐	272
4P-NPD	11 - 54		remote sensing in LED configuration	O	53,238
Alq3	14 - 140	$(0.8 - 7.2)\times10^{-7}$	remote sensing in LED configuration, annihilation, delayed PL	O	44,140, 273
anthracene	610 and 7000 - 20000	$(0.5 - 2)\times10^{-4}$	annihilation, delayed PL, direct imaging	☐▯	246 and 67,248, 274–277
C_{60}	28 - 35		photocurrent, PL quenching	O	200,217

CBP	8.3 - 300	(1.4 - 770) $\times10^{-8}$	remote sensing in LED configuration, PL quenching, photocurrent	○	143,239, 244,278, 279
F8-F6	50	7.9×10^{-6}	annihilation	○	259
F8-PDA	41	4.7×10^{-6}	annihilation	○	259
$Ir(ppy)_3$-cored dendrimers	2 - 10	(8 - 400) $\times10^{-9}$	annihilation	○	243
mCP	16		remote sensing in LED configuration	○	237
naphthalene	35000	3.3×10^{-5}	annihilation, delayed PL	□	272
NPD	6 - 87		photocurrent, remote sensing in tri-layers.	○	240,258
$P(CM\text{-}Ru_x)$	36	(1 - 200) $\times10^{-7}$	PL quenching in bi-layers	○	247
PCBM	21	4.2×10^{-6}	PL quenching in blends	○	200
PdTPPC	30	8×10^{-7}	microwave conductivity	○	242
Pentacene	40 - 800	(1 - 4) $\times10^{-3}$	annihilation, transient absorption, PL quenching, photocurrent	□ ❖	6,9,14, 280
PF		3×10^{-4}	transient absorption	○	260
$Ph_{95}BTD_5$	22	4.7×10^{-6}	PL quenching in blends	○	200
PhLPPP	1700 - 3900	(0.5 - 14) $\times10^{-6}$	transient absorption, annihilation, phosphorescence	○ ▯	101,245

Pt acetylide oligomers		1.8×10^{-4}	transient absorption	o	281
PtOEP	13 - 30		quenching in bi-layers and blends	o	114,200, 254
Pyrene	1200	1.3×10^{-4}	annihilation, delayed PL	☐	282
Rubrene	1000 - 4000		photocurrent, direct imaging	☐	5,187
Stilbene	11000	9×10^{-5}	annihilation, delayed PL	☐	272
Super Yellow PPV	10		quenching in bi-layers	o	241
Tetracene	100 - 400	$(0.1 - 1.6)\times10^{-4}$	photocurrent, annihilation, delayed PL	☐	151,255, 256,283

*2,3,9,10,16,17,23,24-octa-n-dodecyloxymethyl zinc phthalocyanine (**($C_{12}OCH_8)_8$PcZn**), 2,3,6,7,10,11-hexa-n-hexyloxytriphenylene phthalocyanine (**($C_{18}OCH_2$)PcH_2**), 1,4-dibromonaphtalane (1,4-dibromonaphtalane), N,N'-di-1-naphthalenyl-N,N'-diphenyl-[1,1':4',1'':4'',1'''-qua- terphenyl]-4,4'''-diamine (**4P-NPD**), tris(8-hydroxyquinoline) aluminum (**Alq3**), fullerene (**C_{60}**), 4,4'-N,N'-dicarbazole-biphenyl (**CBP**), polyfluorene (**F8-F6**), poly(9,9'-di-n-octylfluorene-ran-N,N'-bis(4-n-butylphenyl)-N,N'-diphenyl-1,4-benzenediamine) (**F8-PDA**), fac-tris(2-phenylpyridine) iridium[III]-cored dendrimers (**Ir(ppy)3-cored dendrimers**), N,N'-dicarbazolyl-3,5-benzene (**mCP**), N, N'-bis(naphthalen-1-yl)- N, N'-bis(phenyl)-benzidine (**NPD**), polycations bearing the Ru moieties (**P(CM-Ru_x**)), [6,6]-phenyl-C_{61}-butyric acid methyl ester (**PCBM**), palladium tetrakis(4-carboxyphenyl)porphyrin (**PdTPPC**), polyfluorene (**PF**), Pt-coordinated polymer (**$Ph_{95}BTD_5$**), diaryl (diphenyl)-substituted ladder-type poly(paraphenylene) (**PhLPPP**) 2,3,7,8,12,13,17,18-octaethyl-21H,23H-porphineplatinum(II) (**PtOEP**), phenyl-substituted poly(p-phenylene vinylene) (Super Yellow PPV).

Acknowledgement. The authors thank the National Science Foundation (DMR-1411349) for the support. T.Q.N. thanks the Camille Dreyfus Teacher Scholar Award.

References

1 Vollhardt, K. P. C. and Schore, N. E., *Organic Chemistry*, W. H. Freeman, Sixth Edition., 2010.

2 Köhler, A. and Bässler, H., *Mater. Sci. Eng. R Rep.*, 2009, **66**, 71–109.

3 Johnson, J. C., Nozik, A. J. and Michl, J., *J. Am. Chem. Soc.*, 2010, **132**, 16302–16303.

4 Congreve, D. N., Lee, J., Thompson, N. J., Hontz, E., Yost, S. R., Reusswig, P. D., Bahlke, M. E., Reineke, S., Voorhis, T. V. and Baldo, M. A., *Science*, 2013, **340**, 334–337.

5 Irkhin, P. and Biaggio, I., *Phys. Rev. Lett.*, 2011, **107**, 017402.

6 Tabachnyk, M., Ehrler, B., Bayliss, S., Friend, R. H. and Greenham, N. C., *Appl. Phys. Lett.*, 2013, **103**, 153302.

7 Walker, B. J., Musser, A. J., Beljonne, D. and Friend, R. H., *Nat. Chem.*, 2013, **5**, 1019–1024.

8 Pensack, R. D., Song, Y., McCormick, T. M., Jahnke, A. A., Hollinger, J., Seferos, D. S. and Scholes, G. D., *J. Phys. Chem. B*, 2014, **118**, 2589–2597.

9 Poletayev, A. D., Clark, J., Wilson, M. W. B., Rao, A., Makino, Y., Hotta, S. and Friend, R. H., *Adv. Mater.*, 2014, **26**, 919–924.

10 Singh, S., Jones, W. J., Siebrand, W., Stoicheff, B. P. and Schneider, W. G., *J. Chem. Phys.*, 1965, **42**, 330–342.

11 Swenberg, C. E. and Stacy, W. T., *Chem. Phys. Lett.*, 1968, **2**, 327–328.

12 Gieseking, B., Schmeiler, T., Müller, B., Deibel, C., Engels, B., Dyakonov, V. and Pflaum, J., *Phys. Rev. B*, 2014, **90**, 205305.

13 Burdett, J. J., Müller, A. M., Gosztola, D. and Bardeen, C. J., *J. Chem. Phys.*, 2010, **133**, 144506.

14 Marciniak, H., Pugliesi, I., Nickel, B. and Lochbrunner, S., *Phys. Rev. B*, 2009, **79**, 235318.

15 Smith, M. B. and Michl, J., *Chem. Rev.*, 2010, **110**, 6891–6936.

16 Smith, M. B. and Michl, J., *Annu. Rev. Phys. Chem.*, 2013, **64**, 361–386.

17 Piland, G. B., Burdett, J. J., Dillon, R. J. and Bardeen, C. J., *J. Phys. Chem. Lett.*, 2014, **5**, 2312–2319.

18 Bardeen, C. J., *Annu. Rev. Phys. Chem.*, 2014, **65**, 127–148.

19 Pope, M. and Swenberg, C. E., *Electronic Processes in Organic Crystals and Polymers*, Oxford University Press, 2nd edn., 1999.

20 Settels, V., Schubert, A., Tafipolski, M., Liu, W., Stehr, V., Topczak, A. K., Pflaum, J., Deibel, C., Fink, R. F., Engel, V. and Engels, B., *J. Am. Chem. Soc.*, 2014, **136**, 9327–9337.

21 Scheidler, M., Lemmer, U., Kersting, R., Karg, S., Riess, W., Cleve, B., Mahrt, R. F., Kurz, H., Bässler, H., Göbel, E. O. and Thomas, P., *Phys. Rev. B*, 1996, **54**, 5536.

22 Ruini, A., Caldas, M. J., Bussi, G. and Molinari, E., *Phys. Rev. Lett.*, 2002, **88**, 206403.

23 Brédas, J.-L., Beljonne, D., Coropceanu, V. and Cornil, J., *Chem. Rev.*, 2004, **104**, 4971–5004.

24 Endo, A., Ogasawara, M., Takahashi, A., Yokoyama, D., Kato, Y. and Adachi, C., *Adv. Mater.*, 2009, **21**, 4802–4806.

25 Blasse, G. and McMillin, D. R., *Chem. Phys. Lett.*, 1980, **70**, 1–3.

26 Adachi, C., *Jpn. J. Appl. Phys.*, 2014, **53**, 060101.

27 Tao, Y., Yuan, K., Chen, T., Xu, P., Li, H., Chen, R., Zheng, C., Zhang, L. and Huang, W., *Adv. Mater.*, 2014, **26**, 7931–7958.

28 Dexter, D. L., *J. Chem. Phys.*, 1953, **21**, 836.

29 Dexter, D. L., Knox, R. S. and Förster, T., *Phys. Status Solidi B*, 1969, **34**, K159–K162.

30 Scholes, G. D., *Annu. Rev. Phys. Chem.*, 2003, **54**, 57–87.

31 Luhman, W. A. and Holmes, R. J., *Adv. Funct. Mater.*, 2011, **21**, 764–771.

32 Koeppe, R. and Sariciftci, N. S., *Photochem. Photobiol. Sci.*, 2006, **5**, 1122–1131.

33 Cleave, V., Yahioglu, G., Barny, P. L., Friend, R. H. and Tessler, N., *Adv. Mater.*, 1999, **11**, 285–288.

34 Cleave, V., Yahioglu, G., Le Barny, P., Hwang, D. H., Holmes, A. B., Friend, R. H. and Tessler, N., *Adv. Mater.*, 2001, **13**, 44–47.

35 Kawamura, Y., Yanagida, S. and Forrest, S. R., *J. Appl. Phys.*, 2002, **92**, 87–93.

36 Gong, X., Lim, S.-H., Ostrowski, J. C., Moses, D., Bardeen, C. J. and Bazan, G. C., *J. Appl. Phys.*, 2004, **95**, 948–953.

37 Kalinowski, J., Stampor, W., Cocchi, M., Virgili, D., Fattori, V. and Di Marco, P., *Chem. Phys.*, 2004, **297**, 39–48.

38 Kawamura, Y., Brooks, J., Brown, J. J., Sasabe, H. and Adachi, C., *Phys. Rev. Lett.*, 2006, **96**, 017404–4.

39 Carvelli, M., Janssen, R. A. J. and Coehoorn, R., *Phys. Rev. B*, 2011, **83**, 075203.

40 Bobbert, P. A., *Nat Mater*, 2010, **9**, 288–290.

41 Lupton, J. M., McCamey, D. R. and Boehme, C., *ChemPhysChem*, 2010, **11**, 3040–3058.

42 Nguyen, T. D., Hukic-Markosian, G., Wang, F., Wojcik, L., Li, X.-G., Ehrenfreund, E. and Vardeny, Z. V., *Nat Mater*, 2010, **9**, 345–352.

43 Monkman, A. P., Rothe, C. and King, S. M., *Proc. IEEE*, 2009, **97**, 1597–1605.

44 Baldo, M. A., O'Brien, D. F., Thompson, M. E. and Forrest, S. R., *Phys. Rev. B*, 1999, **60**, 14422.

45 Wilson, J. S., Dhoot, A. S., Seeley, A. J. A. B., Khan, M. S., Kohler, A. and Friend, R. H., *Nature*, 2001, **413**, 828–831.

46 Cao, Y., Parker, I. D., Yu, G., Zhang, C. and Heeger, A. J., *Nature*, 1999, **397**, 414–417.

47 Yang, C., Vardeny, Z. V., Köhler, A., Wohlgenannt, M., Al-Suti, M. K. and Khan, M. S., *Phys. Rev. B*, 2004, **70**, 241202.

48 Wohlgenannt, M., Tandon, K., Mazumdar, S., Ramasesha, S. and Vardeny, Z. V., *Nature*, 2001, **409**, 494–497.

49 Kersten, S. P., Schellekens, A. J., Koopmans, B. and Bobbert, P. A., *Phys. Rev. Lett.*, 2011, **106**, 197402.

50 Kanno, H., Sun, Y. and Forrest, S. R., *Appl. Phys. Lett.*, 2006, **89**, 143516–3.

51 Sun, Y., Giebink, N. C., Kanno, H., Ma, B., Thompson, M. E. and Forrest, S. R., *Nature*, 2006, **440**, 908–912.

52 Reineke, S., Lindner, F., Schwartz, G., Seidler, N., Walzer, K., Lussem, B. and Leo, K., *Nature*, 2009, **459**, 234–238.

53 Schwartz, G., Reineke, S., Rosenow, T. C., Walzer, K. and Leo, K., *Adv. Funct. Mater.*, 2009, **19**, 1319–1333.

54 Chi, Y. and Chou, P.-T., *Chem. Soc. Rev.*, 2010, **39**, 638–655.

55 Peumans, P., Yakimov, A. and Forrest, S. R., *J. Appl. Phys.*, 2003, **93**, 3693–3723.

56 Heeger, A. J., *Adv. Mater.*, 2014, **26**, 10–28.

57 Dou, L., You, J., Hong, Z., Xu, Z., Li, G., Street, R. A. and Yang, Y., *Adv. Mater.*, 2013, **25**, 6642–6671.

58 Dang, M. T., Hirsch, L., Wantz, G. and Wuest, J. D., *Chem. Rev.*, 2013.

59 Proctor, C. M., Kuik, M. and Nguyen, T.-Q., *Prog. Polym. Sci.*, 2013, **38**, 1941–1960.

60 Nelson, J., *Mater. Today*, 2011, **14**, 462–470.

61 Rand, B. P., Genoe, J., Heremans, P. and Poortmans, J., *Prog. Photovolt. Res. Appl.*, 2007, **15**, 659–676.

62 Walker, B., Kim, C. and Nguyen, T.-Q., *Chem. Mater.*, 2011, **23**, 470–482.

63 Terao, Y., Sasabe, H. and Adachi, C., *Appl. Phys. Lett.*, 2007, **90**, 103515.

64 Menke, S. M., Luhman, W. A. and Holmes, R. J., *Nat. Mater.*, 2013, **12**, 152–157.

65 Lin, J. D. A., Mikhnenko, O. V., van der Poll, T. S., Bazan, G. C. and Nguyen, T.-Q., *Adv. Mater.*, 2015, **27**, 2528–2532.

66 Bjorgaard, J. A. and Köse, M. E., *RSC Adv.*, 2015, **5**, 8432–8445.

67 Ern, V., Suna, A., Tomkiewicz, Y., Avakian, P. and Groff, R. P., *Phys. Rev. B*, 1972, **5**, 3222–3234.

68 Movaghar, B., Ries, B. and Grünewald, M., *Phys. Rev. B*, 1986, **34**, 5574.

69 Beljonne, D., Pourtois, G., Silva, C., Hennebicq, E., Herz, L. M., Friend, R. H., Scholes, G. D., Setayesh, S., Müllen, K. and Brédas, J. L., *Proc. Natl. Acad. Sci.*, 2002, **99**, 10982 –10987.

70 Köhler, A. and Beljonne, D., *Adv. Funct. Mater.*, 2004, **14**, 11–18.

71 Hennebicq, E., Pourtois, G., Scholes, G. D., Herz, L. M., Russell, D. M., Silva, C., Setayesh, S., Grimsdale, A. C., Müllen, K., Brédas, J.-L. and Beljonne, D., *J Am Chem Soc*, 2005, **127**, 4744–4762.

72 Madigan, C. and Bulovic, V., *Phys. Rev. Lett.*, 2006, **96**, 046404–4.

73 Athanasopoulos, S., Hennebicq, E., Beljonne, D. and Walker, A. B., *J Phys Chem C*, 2008, **112**, 11532–11538.

74 Athanasopoulos, S., Emelianova, E. V., Walker, A. B. and Beljonne, D., *Phys. Rev. B Condens. Matter Mater. Phys.*, 2009, **80**, 195209–7.

75 Emelianova, E. V., Athanasopoulos, S., Silbey, R. J. and Beljonne, D., *Phys. Rev. Lett.*, 2010, **104**, 206405.

76 Papadopoulos, T. A., Muccioli, L., Athanasopoulos, S., Walker, A. B., Zannoni, C. and Beljonne, D., *Chem Sci*, 2011, **2**, 1025–1032.

77 Barford, W., Bittner, E. R. and Ward, A., *J. Phys. Chem. A*, 2012, **116**, 10319–10327.

78 Feron, K., Zhou, X., Belcher, W. J. and Dastoor, P. C., *J. Appl. Phys.*, 2012, **111**, 044510–044510–7.

79 Hoffmann, S. T., Athanasopoulos, S., Beljonne, D., Bässler, H. and Köhler, A., *J. Phys. Chem. C*, 2012, **116**, 16371–16383.

80 Valleau, S., Saikin, S. K., Yung, M.-H. and Guzik, A. A., *J. Chem. Phys.*, 2012, **137**, 034109.

81 Athanasopoulos, S., Hoffmann, S. T., Bässler, H., Köhler, A. and Beljonne, D., *J. Phys. Chem. Lett.*, 2013, **4**, 1694–1700.

82 Grisanti, L., Olivier, Y., Wang, L., Athanasopoulos, S., Cornil, J. and Beljonne, D., *Phys. Rev. B*, 2013, **88**, 035450.

83 Li, Z., Zhang, X. and Lu, G., *J. Phys. Condens. Matter*, 2014, **26**, 185006.

84 Stehr, V., Engels, B., Deibel, C. and Fink, R. F., *J. Chem. Phys.*, 2014, **140**, 024503.

85 Tamura, H. and Matsuo, Y., *Chem. Phys. Lett.*, 2014, **598**, 81–85.

86 Fishchuk, I. I., Kadashchuk, A., Hoffmann, S. T., Athanasopoulos, S., Genoe, J., Bässler, H. and Köhler, A., *Phys. Rev. B*, 2013, **88**, 125202.

87 Strzhemechny, M. A., Zloba, D. I., Pyshkin, O. S. and Buravtseva, L. M., *Chem. Phys. Lett.*, 2013, **565**, 61–64.

88 Mikhnenko, O. V., Cordella, F., Sieval, A. B., Hummelen, J. C., Blom, P. W. M. and Loi, M. A., *J. Phys. Chem. B*, 2008, **112**, 11601–11604.

89 Anni, M., Caruso, M. E., Lattante, S. and Cingolani, R., *J. Chem. Phys.*, 2006, **124**, 134707.

90 Bjorklund, T. G., Lim, S.-H. and Bardeen, C. J., *J. Phys. Chem. B*, 2001, **105**, 11970–11977.

91 Arkhipov, V. I., Emelianova, E. V. and Bässler, H., *Chem. Phys. Lett.*, 2004, **383**, 166–170.

92 Hoffmann, S. T., Scheler, E., Koenen, J.-M., Forster, M., Scherf, U., Strohriegl, P., Bässler, H. and Köhler, A., *Phys. Rev. B*, 2010, **81**, 165208.

93 Fennel, F. and Lochbrunner, S., *Phys. Rev. B*, 2012, **85**, 094203.

94 Athanasopoulos, S., Emelianova, E. V., Walker, A. B. and Beljonne, D., 2010, vol. 7722, pp. 772214–772214–8.

95 Bässler, H., *Phys. Status Solidi B*, 1993, **175**, 15–56.

96 Devi, L. S., Al-Suti, M. K., Dosche, C., Khan, M. S., Friend, R. H. and Kohler, A., *Phys. Rev. B Condens. Matter Mater. Phys.*, 2008, **78**, 045210–8.

97 Fishchuk, I. I., Kadashchuk, A., Devi, L. S., Heremans, P., Bassler, H. and Kohler, A., *Phys. Rev. B Condens. Matter Mater. Phys.*, 2008, **78**, 045211–8.

98 Rothe, C. and Monkman, A. P., *Phys. Rev. B*, 2003, **68**, 075208.

99 Romanovskii, Y. V. and Bässler, H., *Chem. Phys. Lett.*, 2000, **326**, 51–57.

100 Lupton, J. M., Pogantsch, A., Piok, T., List, E. J. W., Patil, S. and Scherf, U., *Phys. Rev. Lett.*, 2002, **89**, 167401.

101 Reufer, M., Lagoudakis, P. G., Walter, M. J., Lupton, J. M., Feldmann, J. and Scherf, U., *Phys. Rev. B Condens. Matter Mater. Phys.*, 2006, **74**, 241201–4.

102 Jankus, V., Winscom, C. and Monkman, A. P., *J. Phys. Condens. Matter*, 2010, **22**, 185802.

103 Hoffmann, S. T., Bässler, H., Koenen, J.-M., Forster, M., Scherf, U., Scheler, E., Strohriegl, P. and Köhler, A., *Phys. Rev. B*, 2010, **81**, 115103.

104 Meskers, S. C. J., Hübner, J., Oestreich, M. and Bässler, H., *J. Phys. Chem. B*, 2001, **105**, 9139–9149.

105 Monroe, D., *Phys. Rev. Lett.*, 1985, **54**, 146.

106 Herz, L. M., Silva, C., Grimsdale, A. C., Müllen, K. and Phillips, R. T., *Phys. Rev. B*, 2004, **70**, 165207.

107 Wantz, G., Hirsch, L., Huby, N., Vignau, L., Barrière, A. S. and Parneix, J. P., *J. Appl. Phys.*, 2005, **97**, 034505.

108 Dias, F. B., Kamtekar, K. T., Cazati, T., Williams, G., Bryce, M. R. and Monkman, A. P., *ChemPhysChem*, 2009, **10**, 2096–2104.

109 Zhang, X., Li, Z. and Lu, G., *Phys. Rev. B*, 2011, **84**, 235208.

110 Priestley, R., Walser, A. D. and Dorsinville, R., *Opt. Commun.*, 1998, **158**, 93–96.

111 Liu, X., Zhang, Y. and Forrest, S. R., *Phys. Rev. B*, 2014, **90**, 085201.

112 Jankowiak, R., Ries, B. and Bässler, H., *Phys. Status Solidi B*, 1984, **124**, 363–371.

113 Gaab, K. M. and Bardeen, C. J., *J. Phys. Chem. A*, 2004, **108**, 10801–10806.

114 Lunt, R. R., Giebink, N. C., Belak, A. A., Benziger, J. B. and Forrest, S. R., *J. Appl. Phys.*, 2009, **105**, 053711–7.

115 Menke, S. M. and Holmes, R. J., *Energy Environ. Sci.*, 2014, **7**, 499–512.

116 Lakowicz, J. R., *Principles of Fluorescence Spectroscopy*, Springer, 3rd edn., 2006.

117 Förster, T., *Ann. Phys.*, 1948, **437**, 55–75.

118 Freund, J. A. and Pöschel, T., Stochastic Processes in Physics, Chemistry, and Biology, Springer, 2000.

119 Raisys, S., Kazlauskas, K., Daskeviciene, M., Malinauskas, T., Getautis, V. and Jursenas, S., *J. Mater. Chem. C*, 2014, **2**, 4792–4798.

120 Ward, A. J., Ruseckas, A. and Samuel, I. D. W., *J. Phys. Chem. C*, 2012, **116**, 23931–23937.

121 Lin, J. D. A., Mikhnenko, O. V., Chen, J., Masri, Z., Ruseckas, A., Mikhailovsky, A., Raab, R. P., Liu, J., Blom, P. W. M., Loi, M. A., Garcia-Cervera, C. J., Samuel, I. D. W. and Nguyen, T.-Q., *Mater. Horiz.*, 2014, **1**, 280–285.

122 Hedley, G. J., Ward, A. J., Alekseev, A., Howells, C. T., Martins, E. R., Serrano, L. A., Cooke, G., Ruseckas, A. and Samuel, I. D. W., *Nat. Commun.*, 2013, **4**.

123 Ward, A. J., Ruseckas, A. and Samuel, I. D. W., *J. Phys. Chem. C*, 2012, **116**, 23931–23937.

124 Wang, H., Yue, B., Xie, Z., Gao, B., Xu, Y., Liu, L., Sun, H. and Ma, Y., *Phys. Chem. Chem. Phys.*, 2013, **15**, 3527–3534.

125 Martens, H. C. F., Blom, P. W. M. and Schoo, H. F. M., *Phys. Rev. B*, 2000, **61**, 7489.

126 Markov, D. E. and Blom, P. W. M., *Phys. Rev. B*, 2006, **74**, 085206–5.

127 Haugeneder, A., Neges, M., Kallinger, C., Spirkl, W., Lemmer, U., Feldmann, J., Scherf, U., Harth, E., Gügel, A. and Müllen, K., *Phys. Rev. B*, 1999, **59**, 15346.

128 Siebbeles, L. D. A., Huijser, A. and Savenije, T. J., *J. Mater. Chem.*, 2009, **19**, 6067.

129 Correia, H. M. G., Barbosa, H. M. C., Marques, L. and Ramos, M. M. D., *Comput. Mater. Sci.*, 2013, **75**, 18–23.

130 Shibano, Y., Imahori, H., Sreearunothai, P., Cook, A. R. and Miller, J. R., *J Phys Chem Lett*, 2010, **1**, 1492–1496.

131 Kepler, R. G., Caris, J. C., Avakian, P. and Abramson, E., *Phys. Rev. Lett.*, 1963, **10**, 400–402.

132 Swenberg, C. E., *J. Chem. Phys.*, 1969, **51**, 1753.

133 Suna, A., *Phys. Rev. B*, 1970, **1**, 1716–1739.

134 Partee, J., Frankevich, E. L., Uhlhorn, B., Shinar, J., Ding, Y. and Barton, T. J., *Phys. Rev. Lett.*, 1999, **82**, 3673–3676.

135 Dyakonov, V., Rösler, G., Schwoerer, M. and Frankevich, E. L., *Phys. Rev. B*, 1997, **56**, 3852–3862.

136 Steiner, F., Vogelsang, J. and Lupton, J. M., *Phys. Rev. Lett.*, 2014, **112**, 137402.

137 Merrifield, R. E., *Pure Appl. Chem.*, 1971, **27**, 481–498.

138 Uoyama, H., Goushi, K., Shizu, K., Nomura, H. and Adachi, C., *Nature*, 2012, **492**, 234–238.

139 Jankus, V., Winscom, C. and Monkman, A. P., *Adv. Funct. Mater.*, 2011, **21**, 2522–2526.

140 Luo, Y. and Aziz, H., *J. Appl. Phys.*, 2010, **107**, 094510.

141 Kondakov, D. Y., Pawlik, T. D., Hatwar, T. K. and Spindler, J. P., *J. Appl. Phys.*, 2009, **106**, 124510–7.

142 Baluschev, S., Yakutkin, V., Wegner, G., Minch, B., Miteva, T., Nelles, G. and Yasuda, A., *J. Appl. Phys.*, 2007, **101**, 023101–023101–4.

143 Giebink, N. C., Sun, Y. and Forrest, S. R., *Org. Electron.*, 2006, **7**, 375–386.

144 Laquai, F., Wegner, G., Im, C., Büsing, A. and Heun, S., *J. Chem. Phys.*, 2005, **123**, 074902–074902–6.

145 Rothe, C., King, S. M., Dias, F. and Monkman, A. P., *Phys. Rev. B*, 2004, **70**, 195213.

146 Hayer, A., Bassler, Falk, B. and Schrader, S., *J. Phys. Chem. A*, 2002, **106**, 11045–11053.

147 Hertel, D., Bassler, H., Guentner, R. and Scherf, U., *J. Chem. Phys.*, 2001, **115**, 10007–10013.

148 Hertel, D., Setayesh, S., Nothofer, H. G., Scherf, U., Müllen, K. and Bässler, H., *Adv. Mater.*, 2001, **13**, 65–70.

149 Monkman, A. P., Burrows, H. D., Hamblett, I., Navaratnam, S., Scherf, U. and Schmitt, C., *Chem. Phys. Lett.*, 2000, **327**, 111–116.

150 Landwehr, P., Port, H. and Wolf, H. C., *Chem. Phys. Lett.*, 1996, **260**, 125–129.

151 Aladekomo, J. B., Arnold, S. and Pope, M., *Phys. Status Solidi B*, 1977, **80**, 333–340.

152 Smith, G. C., *Phys. Rev.*, 1968, **166**, 839–847.

153 Priestley, E. B. and Haug, A., *J. Chem. Phys.*, 1968, **49**, 622–629.

154 Mikhnenko, O. V., Blom, P. W. M. and Loi, M. A., *Phys. Chem. Chem. Phys.*, 2011, **13**, 14453–14456.

155 Markov, D. E. and Blom, P. W. M., *Appl. Phys. Lett.*, 2005, **87**, 233511–3.

156 Mikhnenko, O. V., Cordella, F., Sieval, A. B., Hummelen, J. C., Blom, P. W. M. and Loi, M. A., *J. Phys. Chem. B*, 2009, **113**, 9104–9109.

157 Loi, M. A., Mura, A., Bongiovanni, G., Cai, Q., Martin, C., Chandrasekhar, H. R., Chandrasekhar, M., Graupner, W. and Garnier, F., *Phys. Rev. Lett.*, 2001, **86**, 732.

158 Hess, B. C., Kanner, G. S. and Vardeny, Z., *Phys. Rev. B*, 1993, **47**, 1407.

159 Tikhoplav, R. K. and Hess, B. C., *Synth. Met.*, 1999, **101**, 236–237.

160 Lunt, R. R., Benziger, J. B. and Forrest, S. R., *Adv. Mater.*, 2010, **22**, 1233–1236.

161 Brabec, C. J., Zerza, G., Cerullo, G., De Silvestri, S., Luzzati, S., Hummelen, J. C. and Sariciftci, S., *Chem. Phys. Lett.*, 2001, **340**, 232–236.

162 Wang, H., Wang, H.-Y., Gao, B.-R., Wang, L., Yang, Z.-Y., Du, X.-B., Chen, Q.-D., Song, J.-F. and Sun, H.-B., *Nanoscale*, 2011, **3**, 2280.

163 Cook, S., Liyuan, H., Furube, A. and Katoh, R., *J. Phys. Chem. C*, 2010, **114**, 10962–10968.

164 Masuda, K., Ikeda, Y., Ogawa, M., Benten, H., Ohkita, H. and Ito, S., *ACS Appl. Mater. Interfaces*, 2010, **2**, 236–245.

165 Cook, S., Furube, A., Katoh, R. and Han, L., *Chem. Phys. Lett.*, 2009, **478**, 33–36.

166 Shaw, P. E., Ruseckas, A. and Samuel, I. D. W., *Adv. Mater.*, 2008, **20**, 3516–3520.

167 Goh, C., Scully, S. R. and McGehee, M. D., *J. Appl. Phys.*, 2007, **101**, 114503.

168 Lewis, A. J., Ruseckas, A., Gaudin, O. P. M., Webster, G. R., Burn, P. L. and Samuel, I. D. W., *Org. Electron.*, 2006, **7**, 452–456.

169 Scully, S. R. and McGehee, M. D., *J. Appl. Phys.*, 2006, **100**, 034907–5.

170 Wu, Y., Zhou, Y. C., Wu, H. R., Zhan, Y. Q., Zhou, J., Zhang, S. T., Zhao, J. M., Wang, Z. J., Ding, X. M. and Hou, X. Y., *Appl. Phys. Lett.*, 2005, **87**, 044104–3.

171 Markov, D. E., Tanase, C., Blom, P. W. M. and Wildeman, J., *Phys. Rev. B*, 2005, **72**, 045217–6.

172 Markov, D. E., Hummelen, J. C., Blom, P. W. M. and Sieval, A. B., *Phys. Rev. B*, 2005, **72**, 045216–5.

173 Markov, D. E., Amsterdam, E., Blom, P. W. M., Sieval, A. B. and Hummelen, J. C., *J. Phys. Chem. A*, 2005, **109**, 5266–5274.

174 Lüer, L., Egelhaaf, H.-J., Oelkrug, D., Cerullo, G., Lanzani, G., Huisman, B.-H. and de Leeuw, D., *Org. Electron.*, 2004, **5**, 83–89.

175 Kroeze, J. E., Savenije, T. J., Vermeulen, M. J. W. and Warman, J. M., *J. Phys. Chem. B*, 2003, **107**, 7696–7705.

176 Yang, C. L., Tang, Z. K., Ge, W. K., Wang, J. N., Zhang, Z. L. and Jian, X. Y., *Appl. Phys. Lett.*, 2003, **83**, 1737–1739.

177 Stubinger, T. and Brutting, W., *J. Appl. Phys.*, 2001, **90**, 3632–3641.

178 Theander, M., Yartsev, A., Zigmantas, D., Sundström, V., Mammo, W., Andersson, M. R. and Inganäs, O., *Phys. Rev. B*, 2000, **61**, 12957.

179 Gregg, B. A., Sprague, J. and Peterson, M. W., *J. Phys. Chem. B*, 1997, **101**, 5362–5369.

180 Halls, J. J. M., Pichler, K., Friend, R. H., Moratti, S. C. and Holmes, A. B., *Appl. Phys. Lett.*, 1996, **68**, 3120–3122.

181 Zhou, Y. C., Wu, Y., Ma, L. L., Zhou, J., Ding, X. M. and Hou, X. Y., *J. Appl. Phys.*, 2006, **100**, 023712–5.

182 Leow, C., Ohnishi, T. and Matsumura, M., *J. Phys. Chem. C*, 2013.

183 Köse, M. E., Graf, P., Kopidakis, N., Shaheen, S. E., Kim, K. and Rumbles, G., *ChemPhysChem*, 2009, **10**, 3285–3294.

184 Rim, S.-B., Fink, R. F., Schöneboom, J. C., Erk, P. and Peumans, P., *Appl. Phys. Lett.*, 2007, **91**, 173504.

185 Breyer, C., Vogel, M., Mohr, M., Johnev, B. and Fostiropoulos, K., *Phys. Status Solidi B*, 2006, **243**, 3176 – 318.

186 Mani, A., Schoonman, J. and Goossens, A., *J. Phys. Chem. B*, 2005, **109**, 4829–4836.

187 Najafov, H., Lee, B., Zhou, Q., Feldman, L. C. and Podzorov, V., *Nat Mater*, 2010, **9**, 938–943.

188 Wei, G., Lunt, R. R., Sun, K., Wang, S., Thompson, M. E. and Forrest, S. R., *Nano Lett*, 2010, **10**, 3555–3559.

189 Bergemann, K. J. and Forrest, S. R., *Appl. Phys. Lett.*, 2011, **99**, 243303.

190 Mikhnenko, O. V., Azimi, H., Scharber, M., Morana, M., Blom, P. W. M. and Loi, M. A., *Energy Environ. Sci.*, 2012, **5**, 6960.

191 Groff, L. C., Wang, X. and McNeill, J. D., *J. Phys. Chem. C*, 2013, **117**, 25748–25755.

192 Bruno, A., Reynolds, L. X., Dyer-Smith, C., Nelson, J. and Haque, S. A., *J. Phys. Chem. C*, 2013, **117**, 19832–19838.

193 Donker, H., Koehorst, R. B. M. and Schaafsma, T. J., *J. Phys. Chem. B*, 2005, **109**, 17031–17037.

194 http://mikhnenko.com/eDiffusion/, .

195 Mikhnenko, O. V., Kuik, M., Lin, J., van der Kaap, N., Nguyen, T.-Q. and Blom, P. W. M., *Adv. Mater.*, 2014, **26**, 1912–1917.

196 Geddes, C. D., *Meas. Sci. Technol.*, 2001, **12**, R53–R88.

197 Hartmann, P. and Trettnak, W., *Anal. Chem.*, 1996, **68**, 2615–2620.

198 Morana, M., Azimi, H., Dennler, G., Egelhaaf, H.-J., Scharber, M., Forberich, K., Hauch, J., Gaudiana, R., Waller, D., Zhu, Z., Hingerl, K., van Bavel, S. S., Loos, J. and Brabec, C. J., *Adv. Funct. Mater.*, 2010, **20**, 1180–1188.

199 Ruseckas, A., Shaw, P. E. and Samuel, I. D. W., *Dalton Trans.*, 2009, 10040.

200 Hsu, H.-Y., Vella, J. H., Myers, J. D., Xue, J. and Schanze, K. S., *J. Phys. Chem. C*, 2014, **118**, 24282–24289.

201 Tamai, Y., Matsuura, Y., Ohkita, H., Benten, H. and Ito, S., *J. Phys. Chem. Lett.*, 2014, **5**, 399–403.

202 Shin, H.-Y., Woo, J. H., Gwon, M. J., Barthelemy, M., Vomir, M., Muto, T., Takaishi, K., Uchiyama, M., Hashizume, D., Aoyama, T., Kim, D.-W., Yoon, S., Bigot, J.-Y., Wu, J. W. and Ribierre, J. C., *Phys. Chem. Chem. Phys.*, 2013, **15**, 2867–2872.

203 Marciniak, H., Li, X.-Q., Würthner, F. and Lochbrunner, S., *J. Phys. Chem. A*, 2011, **115**, 648–654.

204 Shaw, P. E., Ruseckas, A., Peet, J., Bazan, G. C. and Samuel, I. D. W., *Adv. Funct. Mater.*, 2010, **20**, 155–161.

205 Ruseckas, A., Ribierre, J. C., Shaw, P. E., Staton, S. V., Burn, P. L. and Samuel, I. D. W., *Appl. Phys. Lett.*, 2009, **95**, 183305–3.

206 Engel, E., Leo, K. and Hoffmann, M., *Chem. Phys.*, 2006, **325**, 170–177.

207 Markovitsi, D., Thu Hoa Tran Thi, ., Briois, V., Simon, J. and Ohta, K., *J. Am. Chem. Soc.*, 1988, **110**, 2001–2002.

208 Markovitsi, D. and Lécuyer, I., *Chem. Phys. Lett.*, 1988, **149**, 330–333.

209 Kroeze, J. E., Koehorst, R. B. M. and Savenije, T. J., *Adv. Funct. Mater.*, 2004, **14**, 992–998.

210 Fravventura, M. C., Hwang, J., Suijkerbuijk, J. W. A., Erk, P., Siebbeles, L. D. A. and Savenije, T. J., *J. Phys. Chem. Lett.*, 2012, **3**, 2367–2373.

211 Huijser, A., Savenije, T. J., Kroeze, J. E. and Siebbeles, L. D. A., *J. Phys. Chem. B*, 2005, **109**, 20166–20173.

212 Huijser, A., Savenije, T. J., Kotlewski, A., Picken, S. J. and Siebbeles, L. D. A., *Adv. Mater.*, 2006, **18**, 2234–2239.

213 Huijser, A., Savenije, T. J., Meskers, S. C. J., Vermeulen, M. J. W. and Siebbeles, L. D. A., *J. Am. Chem. Soc.*, 2008, **130**, 12496–12500.

214 Huijser, A., Suijkerbuijk, B. M. J. M., Klein Gebbink, R. J. M., Savenije, T. J. and Siebbeles, *J. Am. Chem. Soc.*, 2008, **130**, 2485–2492.

215 Pettersson, L. A. A., Roman, L. S. and Inganäs, O., *J. Appl. Phys.*, 1999, **86**, 487–496.

216 Bulovic, V. and Forrest, S. R., *Chem. Phys. Lett.*, 1995, **238**, 88–92.

217 Qin, D., Gu, P., Dhar, R. S., Razavipour, S. G. and Ban, D., *Phys. Status Solidi A*, 2011, **208**, 1967–1971.

218 Guide, M., Lin, J. D. A., Proctor, C. M., Chen, J., García-Cervera, C. and Nguyen, T.-Q., *J. Mater. Chem. A*, 2014, **2**, 7890–7896.

219 Ichikawa, M., *Thin Solid Films*, 2013, **527**, 239–243.

220 Toušek, J., Toušková, J., Remeš, Z., Čermák, J., Kousal, J., Kindl, D. and Kuřitka, I., *Chem. Phys. Lett.*, 2012, **552**, 49–52.

221 Kozub, D. R., Vakhshouri, K., Kesava, S. V., Wang, C., Hexemer, A. and Gomez, E. D., *Chem. Commun.*, 2012, **48**, 5859.

222 Hofmann, S., Rosenow, T. C., Gather, M. C., Lüssem, B. and Leo, K., *Phys. Rev. B*, 2012, **85**, 245209.

223 Kurrle, D. and Pflaum, J., *Appl. Phys. Lett.*, 2008, **92**, 133306.

224 Kerp, H. R., Donker, H., Koehorst, R. B. M., Schaafsma, T. J. and van Faassen, E. E., *Chem. Phys. Lett.*, 1998, **298**, 302–308.

225 Kozyreff, G., Urbanek, D. C., Vuong, L. T., Silleras, O. N. and Martorell, J., *Opt. Express*, 2013, **21**, A336–A354.

226 Liang, Z. and Gregg, B. A., *Adv. Mater.*, 2012, **24**, 3258–3262.

227 Nicolai, H. T., Kuik, M., Wetzelaer, G. A. H., de Boer, B., Campbell, C., Risco, C., Brédas, J. L. and Blom, P. W. M., *Nat. Mater.*, 2012, **11**, 882.

228 Yost, S. R., Hontz, E., Yeganeh, S. and Van Voorhis, T., *J. Phys. Chem. C*, 2012, **116**, 17369–17377.

229 Menke, S. M., Lindsay, C. D. and Holmes, R. J., *Appl. Phys. Lett.*, 2014, **104**, 243302.

230 Yang, J., Zhu, F., Yu, B., Wang, H. and Yan, D., *Appl. Phys. Lett.*, 2012, **100**, 103305–103305–4.

231 Sim, M., Shin, J., Shim, C., Kim, M., Jo, S. B., Kim, J.-H. and Cho, K., *J. Phys. Chem. C*, 2013.

232 Kazzaz, A. A. and Zahlan, A. B., *Phys. Rev.*, 1961, **124**, 90–95.

233 Topczak, A. K., Roller, T., Engels, B., Brütting, W. and Pflaum, J., *Phys. Rev. B*, 2014, **89**, 201203.

234 Mikhnenko, O. V., Lin, J., Shu, Y., Anthony, J. E., Blom, P. W. M., Nguyen, T.-Q. and Loi, M. A., *Phys. Chem. Chem. Phys.*, 2012, **14**, 14196–14201.

235 Ko, S., Kim, D. H., Ayzner, A. L., Mannsfeld, S. C. B., Verploegen, E., Nardes, A. M., Kopidakis, N., Toney, M. F. and Bao, Z., *Chem. Mater.*, 2015, **27**, 1223–1232.

236 Ortiz, A. L., Collier, G. S., Marin, D. M., Kassel, J. A., Ivins, R. J., Grubich, N. G. and Walter, M. G., *J. Mater. Chem. C*, 2015, **3**, 1243–1249.

237 Zhang, W., Yu, J., Wen, W. and Jiang, Y., *J. Lumin.*, 2011, **131**, 1260–1263.

238 Wünsche, J., Reineke, S., Lüssem, B. and Leo, K., *Phys. Rev. B*, 2010, **81**, 245201.

239 Lebental, M., Choukri, H., Chenais, S., Forget, S., Siove, A., Geffroy, B. and Tutis, E., *Phys. Rev. B Condens. Matter Mater. Phys.*, 2009, **79**, 165318–13.

240 Luhman, W. A. and Holmes, R. J., *Appl. Phys. Lett.*, 2009, **94**, 153304–3.

241Rand, B. P., Schols, S., Cheyns, D., Gommans, H., Girotto, C., Genoe, J., Heremans, P. and Poortmans, J., *Org. Electron.*, 2009, **10**, 1015–1019.

242 Kroeze, J. E., Savenije, T. J., Candeias, L. P., Warman, J. M. and Siebbeles, L. D. A., *Sol. Energy Mater. Sol. Cells*, 2005, **85**, 189–203.

243 Namdas, E. B., Ruseckas, A., Samuel, I. D. W., Lo, S.-C. and Burn, P. L., *Appl. Phys. Lett.*, 2005, **86**, 091104–3.

244 Matsusue, N., Ikame, S., Suzuki, Y. and Naito, H., *J. Appl. Phys.*, 2005, **97**, 123512–5.

245 Samiullah, M., Moghe, D., Scherf, U. and Guha, S., *Phys. Rev. B*, 2010, **82**, 205211.

246 Akselrod, G. M., Deotare, P. B., Thompson, N. J., Lee, J., Tisdale, W. A., Baldo, M. A., Menon, V. M. and Bulović, V., *Nat. Commun.*, 2014, **5**.

247 Fushimi, T., Oda, A., Ohkita, H. and Ito, S., *J. Phys. Chem. B*, 2004, **108**, 18897–18902.

248 Avakian, P. and Merrifield, R. E., *Phys. Rev. Lett.*, 1964, **13**, 541–543.

249 Johnson, R. C., Merrifield, R. E., Avakian, P. and Flippen, R. B., *Phys. Rev. Lett.*, 1967, **19**, 285–287.

250 Wu, C., Djurovich, P. I. and Thompson, M. E., *Adv. Funct. Mater.*, 2009, **19**, 3157–3164.

251Baldo, M. A., Adachi, C. and Forrest, S. R., *Phys. Rev. B*, 2000, **62**, 10967.

252 D'Andrade, B. w., Thompson, M. e. and Forrest, S. r., *Adv. Mater.*, 2002, **14**, 147–151.

253 Giebink, N. C. and Forrest, S. R., *Phys. Rev. B Condens. Matter Mater. Phys.*, 2008, **77**, 235215–9.

254 Shao, Y. and Yang, Y., *Adv. Mater.*, 2005, **17**, 2841–2844.

255 Vaubel, G. and Kallmann, H., *Phys. Status Solidi B*, 1969, **35**, 789–792.

256 Hofberger, W. and Bässler, H., *Phys. Status Solidi B*, 1975, **69**, 725–730.

257Rand, B. P., Girotto, C., Mityashin, A., Hadipour, A., Genoe, J. and Heremans, P., *Appl. Phys. Lett.*, 2009, **95**, 173304–3.

258 Mikhnenko, O. V., Ruiter, R., Blom, P. W. M. and Loi, M. A., *Phys Rev Lett*, 2012, **108**, 137401.

259 Tamai, Y., Ohkita, H., Benten, H. and Ito, S., *Chem. Mater.*, 2014, **26**, 2733–2742.

260 Sreearunothai, P., Estrada, A., Asaoka, S., Kowalczyk, M., Jang, S., Cook, A. R., Preses, J. M. and Miller, J. R., *J Phys Chem C*, 2011, **115**, 19569–19577.

261 Stich, D., Späth, F., Kraus, H., Sperlich, A., Dyakonov, V. and Hertel, T., *Nat. Photonics*, 2014, **8**, 139–144.

262 Blanzat, B., Barthou, C., Tercier, N., Andre, J. J. and Simon, J., *J. Am. Chem. Soc.*, 1987, **109**, 6193–6194.

263 Choong, V.-E., Park, Y., Gao, Y., Mason, M. G. and Tang, C. W., *J. Vac. Sci. Technol. A*, 1998, **16**, 1838–1841.

264 Burin, A. L. and Ratner, M. A., *J. Phys. Chem. A*, 2000, **104**, 4704–4710.

265 Piersimoni, F., Cheyns, D., Vandewal, K., Manca, J. V. and Rand, B. P., *J. Phys. Chem. Lett.*, 2012, **3**, 2064–2068.

266 Rothberg, L. J., Yan, M., Papadimitrakopoulos, F., Galvin, M. E., Kwock, E. W. and Miller, T. M., *Synth. Met.*, 1996, **80**, 41–58.

267 Healy, A. T., Boudouris, B. W., Frisbie, C. D., Hillmyer, M. A. and Blank, D. A., *J. Phys. Chem. Lett.*, 2013, **4**, 3445–3449.

268 Wang, Y., Ohkita, H., Benten, H. and Ito, S., *ChemPhysChem*, 2015, n/a–n/a.

269 Wang, Y., Benten, H., Ohara, S., Kawamura, D., Ohkita, H. and Ito, S., *ACS Appl. Mater. Interfaces*, 2014, **6**, 14108–14115.

270 Zaikowski, L., Mauro, G., Bird, M., Karten, B., Asaoka, S., Wu, Q., Cook, A. R. and Miller, J. R., *J. Phys. Chem. B*, 2014.

271 Donker, H., van Hoek, A., van Schaik, W., Koehorst, R. B. M., Yatskou, M. M. and Schaafsma, T. J., *J. Phys. Chem. B*, 2005, **109**, 17038–17046.

272 Ern, V., *J. Chem. Phys.*, 1972, **56**, 6259–6260.

273 Baldo, M. A. and Forrest, S. R., *Phys. Rev. B*, 2000, **62**, 10958.

274 Ern, V., Avakian, P. and Merrifield, R. E., *Phys. Rev.*, 1966, **148**, 862–867.

275 Levine, M., Jortner, J. and Szöke, A., *J. Chem. Phys.*, 1966, **45**, 1591–1604.

276 Avakian, P., Ern, V., Merrifield, R. E. and Suna, A., *Phys. Rev.*, 1968, **165**, 974–980.

277 Ern, V., *Phys. Rev. Lett.*, 1969, **22**, 343–345.

278 D'Andrade, B. W., Holmes, R. J. and Forrest, S. R., *Adv. Mater.*, 2004, **16**, 624–628.

279 Zhou, Y. C., Ma, L. L., Zhou, J., Ding, X. M. and Hou, X. Y., *Phys. Rev. B*, 2007, **75**, 132202.

280 Rao, A., Wilson, M. W. B., Hodgkiss, J. M., Albert-Seifried, S., Bässler, H. and Friend, R. H., *J. Am. Chem. Soc.*, 2010, **132**, 12698–12703.

281 Keller, J. M., Glusac, K. D., Danilov, E. O., McIlroy, S., Sreearuothai, P., R. Cook, A., Jiang, H., Miller, J. R. and Schanze, K. S., *J. Am. Chem. Soc.*, 2011, **133**, 11289–11298.

282 Arnold, S., Fave, J. L. and Schott, M., *Chem. Phys. Lett.*, 1974, **28**, 412–417.
283 Alfano, R. R., Shapiro, S. L. and Pope, M., *Opt. Commun.*, 1973, **9**, 388–391.